

MEASUREMENTS OF VOLATILE ORGANIC COMPOUNDS IN DIESEL AND
GASOLINE EXHAUST USING PROTON-TRANSFER REACTION MASS
SPECTROMETRY

By
MYLENE GUENERON

A Thesis submitted in partial fulfillment of the
requirements for the degree of
MASTER OF SCIENCE IN ENVIRONMENTAL ENGINEERING

WASHINGTON STATE UNIVERSITY
Department of Civil and Environmental Engineering

DECEMBER 2012

To the Faculty of Washington State University:

The members of the Committee appointed to examine the
thesis of MYLENE GUENERON, M.S. find it satisfactory and recommend that
it be accepted.

Tom Jobson, PhD., Chair

Tim VanReken, PhD.

Heping Liu, PhD.

ACKNOWLEDGMENTS

I would like to thank some people that have been there for me during my master and helped me go through this great experience.

First of all, I am grateful for Tom Jobson who has been an amazing advisor to work for. He was available, comprehensive, patient and knows how to stimulate his students in their work. I would also like to thank the people that I had worked with in the laboratory: especially Matt Erickson who taught me patiently how to use the PTR-MS, Graham VanderSchelden who is very easy to work with, Will Wallace who always had constructive comments on my work, and last but not the least I would like to particularly acknowledge Claudia Toro who not only helped me go through my thesis with wise advices but also she was my friend since my first day in the program. I would also like to thank Courtney Herring for her nice collaboration on the LRRI field experiment.

I also thank my office mates from LAR that gave me great support with a special mention for Jinshu Chi, also Celia Faiola and Tsenguel Nergui.

I am also thankful for my family and friends who were moral support during my studies.

Finally I would like to thank the University of Washington Clean Air Research Center (CCAR), EPA grant #RD83479601, for its funding.

MEASUREMENTS OF VOLATILE ORGANIC COMPOUNDS IN DIESEL AND
GASOLINE EXHAUST USING PROTON-TRANSFER REACTION MASS
SPECTROMETRY

Abstract

by MYLENE GUENERON, M.S.
Washington State University
DECEMBER 2012

Chair: Tom Jobson

A Proton Transfer Reaction Mass Spectrometer (PTR-MS) was used to measure the abundance of organics in diesel and gasoline engine exhaust mixtures as part of a health effects study conducted at the Lovelace Respiratory Research Institute. To aid in the interpretation of PTR-MS mass spectra of exhaust mixtures, laboratory experiments were conducted to better understand the sensitivity and fragmentation patterns for a series of alkyl substituted monoaromatics and polyaromatic hydrocarbons found in exhaust. Monoaromatic compound fragmentation was examined for drift tube conditions of 80, 100, 120, and 150 Td. It was observed that compounds with ethyl or isopropyl groups attached to a benzene ring are susceptible to fragmentation and can therefore produce positive inferences in the measurement of benzene and toluene. The sensitivity of the PTR-MS to the PAH compounds acenaphthylene, acenaphthene, and biphenyl was determined by preparing standards in dichloromethane and using a syringe pump to dynamically dilute evaporated standard solutions into a flow of hot dry nitrogen gas. The sensitivity was found to be 3.1 ± 0.3 , 3.2 ± 0.3 , and 3.2 ± 0.6 Hz per MHz H_3O^+

per ppbV respectively at the 80 Td drift tube condition. The PAH compounds did not fragment and therefore can be monitored at their M+1 ion. The mass spectrums of diesel and gasoline exhaust were quite similar with a few exceptions. While the gasoline exhaust had much higher concentrations of volatile organic compounds (VOCs), the abundance of compounds relative to benzene was similar. Low engine loads had the highest concentrations for both engines. The data show some evidence that in diesel and gasoline exhaust mixtures with high particle mass concentrations, PAH compounds partition from the gas phase to the particle phase and may offer an explanation as to why gasoline and diesel exhaust mixtures are more toxic than either alone.

CONTENTS

Acknowledgments	iii
Abstract	iv
List of Tables	viii
List of Figures	x
1 Introduction	1
1.1 Vehicle emissions: effect on human health	1
1.2 Diesel and gasoline composition	3
1.3 Partitioning hypothesis	5
2 Experimental Setup	10
2.1 PTR-MS	10
2.1.1 PTR-MS measurement principle	10
2.1.2 Intermediate volatile organic compounds (IVOCs) measurements	16
2.2 Dynamic Dilution System	18
2.2.1 Injection of test mixtures	18
2.2.2 Calculations of test mixture molar mixing ratios	19
2.2.3 PTR-MS calibration with a compressed gas standard	22
3 Experimental Results	25
3.1 Dynamic Dilution System	25
3.1.1 Accuracy of the syringe pump infusion rate	25
3.1.2 Aromatic Sensitivities	26
3.1.3 Accuracy of the dynamic dilution system	29
3.1.4 PAH sensitivities	37
3.2 Fragmentation: dissociative proton transfer reactions	39
3.2.1 Fragmentation Patterns of Aromatic Compounds	39
3.2.1.1 Monocyclic aromatic hydrocarbons	43

3.2.1.2	Naphthalenes	48
3.2.1.3	PAHs	52
3.2.1.4	Biphenyl	52
3.2.2	Fragmentation Pattern Summary	53
4	LRRI	61
4.1	Purpose of the study	61
4.2	Exposure chamber experimental set up	62
4.3	PTR-MS Sampling of Chambers	66
4.3.1	Fuels composition and comparison to engine exhaust	69
4.3.2	Comparison of gasoline and diesel exhaust composition	74
4.3.3	Particle and engine loading variations	75
4.3.3.1	Diesel	75
4.3.3.2	Gasoline	77
4.3.3.3	Mixture with variation in the gas and particles loadings	80
5	Conclusions	83
	References	88

LIST OF TABLES

2.1	Mixing Ratios of VOCs in the PTR-MS Calibration Standard tank	24
3.1	Results on the accuracy of the syringe pump infusion rate	26
3.2	Final aromatic sensitivities at Td80 and Td120	28
3.3	Ranges of expected mixing ratio for benzene, toluene, p-xylene and 1,3,5-trimethylbenzene.	29
3.4	PAHs sensitivities at Td80	38
3.5	List of compounds tested for fragmentation.	41
3.6	Fragmentation	60
4.1	Engine load conditions	64
4.2	Experiments Summary	65
4.3	Ions measured with the PTR-MS during the exposure chamber exper- iment	69

LIST OF FIGURES

1.1	Illustration of the influence of the aerosol mass concentration in the partitioning process.	6
1.2	Lipid Peroxidal Response to Different Mixing Exposure	8
1.3	Illustration of the repartitioning hypothesis in mixtures of diesel and gasoline exhausts.	9
2.1	Schematic of the PTR-MS	13
2.2	PTR-MS mass spectrum of a calibration tank experiment at Td80 . .	14
2.3	Four modes of the cold trap	15
2.4	Schematic of the VOC/IVOC system	17
2.5	Diagram of the dynamic dilution system setup for making ppbv test gas mixtures from liquid chemicals.	20
2.6	Temperature difference in the dynamic dilution system between T_1 and T_2	20
2.7	Diagram of the dynamic dilution system setup for calibration tests using a compressed gas standard.	23
3.1	Comparison of the averaged sensitivities between the new tank and old tank.	27
3.2	1,3,5-trimethylbenzene: measured concentration against expected concentration for a temperature range of $[T=30^{\circ}\text{C} : T=70^{\circ}\text{C}]$	33
3.3	P-xylene: measured concentration against expected concentration for a temperature range of $[T=30^{\circ}\text{C} : T=70^{\circ}\text{C}]$	34
3.4	Toluene: measured concentration against expected concentration for a temperature range of $[T=30^{\circ}\text{C} : T=70^{\circ}\text{C}]$	35
3.5	Benzene: measured concentration against expected concentration for a temperature range of $[T_{room} : T=70^{\circ}\text{C}]$	36
3.6	Upper limit of vapor pressures	38
3.7	Mass spectra of the dichloromethane at Td80 and Td150	43
3.8	Fragmentation of naphthalene: barscan	49
3.9	Fragmentation 1,2-dihydronaphthalene: barscan	51

3.10	Fragmentation acenaphthylene: barscan	54
3.11	Fragmentation acenaphthene: barscan	55
3.12	Fragmentation biphenyl: barscan	56
3.13	Fragmentation abundance (%)	57
3.14	Fragmentation abundance (%) (continued)	58
3.15	Fragmentation abundance (%) (continued)	59
4.1	General plumbing schematic of the exposure chamber measurements .	63
4.2	Pictures of the chamber exposure connection with the PTR-MS. . . .	68
4.3	PTR-MS mass spectra of diesel exhaust and diesel fuel.	72
4.4	PTR-MS mass spectra of gasoline engine exhaust and gasoline fuel. .	73
4.5	Organics abundance relative to benzene for diesel and gasoline exhaust.	74
4.6	Impact of diesel particle loading on organics abundance at typical engine loading (total organic abundance).	77
4.7	Impact of diesel particle loading on organics abundance at typical engine loading.	78
4.8	Impact of diesel engine loading on the organic abundance in a diesel only mixture, at a constant particle loading	78
4.9	Impact of diesel engine loading on the organic abundance in a gasoline and diesel mixture, at a constant particle loading for both diesel and gasoline	79
4.10	Impact of particle loading and engine loading variations for gasoline only mixtures.	80
4.11	Impact of the increase in the fraction of diesel on the organic abundance of a mixture (PTR-MS)	81
4.12	Impact of the increase in the fraction of diesel on the organic abundance of a mixture (HR-ToF-AMS)	82

CHAPTER 1. INTRODUCTION

1.1 Vehicle emissions: effect on human health

Vehicles emissions are a major source of air pollution in the United States. According to the US Environmental Protection Agency's (EPA) 2008 National Emissions Inventory, roadway vehicles emissions contribute 17% of the nation's total VOC emissions from anthropogenic sources, 40% of the carbon monoxide (CO) emissions, 38% of the oxides of nitrogen (NO_x) emissions, and 5% of PM_{2.5} (particulate matter with a diameter less than 2.5 μ m) emissions. Since vehicle emissions are concentrated in urban areas, the relative importance of these emissions to an urban area emission inventory can be much larger than the national average. Heavy duty diesel vehicles are the most important roadway source of PM_{2.5} while gasoline vehicles are the most important source of VOCs and CO. NO₂, CO, and PM_{2.5} are criteria air pollutants and ambient concentrations are regulated by the EPA because of their effects on human health. To reduce exposure to these pollutants vehicle emissions rates of VOCs, CO, NO_x and PM_{2.5} are also regulated by the EPA. Diesel and gasoline vehicle exhaust are known to have carcinogenic or respiratory tract irritation effects. Diesel engine PM_{2.5} emissions are now recognized as being carcinogenic by the World Health Organization.

Pope and Dockery (1), wrote a critical review of several studies on the specific effect of PM on health. While $\text{PM}_{2.5}$ and PM_{10} mass concentrations are both regulated by the Environmental Protection Agency with a limitation of $35\mu\text{g m}^{-3}$ and $150\mu\text{g m}^{-3}$ for 24 hours respectively, health effects may be due to exposure to small submicron sized particles. There are different sizes of particulate matter: coarse particles with an aerodynamic diameter greater than $2.5\mu\text{m}$, fine particles with an aerodynamic diameter less than $2.5\mu\text{m}$ ($\text{PM}_{2.5}$), and ultrafine particles with an aerodynamic diameter less than $0.1\mu\text{m}$ ($\text{PM}_{0.1}$). The human immune system is complex and very reactive to cellular intrusion of any unknown substance. When particles enter the cellular layer, the immune system starts up and immune responses can be observed and quantified. When breathing in gasoline and diesel exhausts a subject inhales these gases and particles. The particles can deposit inside the respiratory tract. Particles will settle at different depths inside the respiratory system depending on their size. Larger particles (larger than $10\mu\text{m}$) get stuck in the upper respiratory tract in the oral cavity, nasal passage, and trachea. Fine and ultrafine particles can make their way deeper to the alveolar region where gas exchange takes place and can even pass through cell membranes. Particles thus can deliver chemicals to different places in the respiratory tract and these chemicals are taken up by the body. Mortality increases with time of exposure to elevated PM concentrations. PM exposure is likely to lead to cardiovascular mortality, pulmonary inflammation, subclinical chronic inflammatory lung injury, and arterial vasoconstriction (1–10).

1.2 Diesel and gasoline composition

There is a special interest in organic compounds from vehicle exhaust as these compounds are chemically reactive and contribute to ozone and $\text{PM}_{2.5}$ formation in urban areas (11–13). The organic compounds can be directly emitted in the condensed phase as primary organic aerosols (POA) or in the gaseous phase as VOCs that can further oxidize in the atmosphere to form less volatile compounds called semi-volatile organic compounds (SVOCs) that can condense onto airborne particles creating secondary organic aerosols (SOA). In urban areas POAs are mainly emitted from meat cooking, paved road dust, fireplaces and vehicle emissions (14). Many VOC present in the gas phase have been identified as potential sources of SOA (15–18). To study vehicles emissions there are two main types of experiments, the dynamometer studies and the on-road studies that typically make measurements from traffic tunnels. The dynamometer studies provide precise results of emissions factors, but are not as representative of the actual emissions as the on-road studies. The latter are more realistic but the test conditions are not well controlled. Standard methods for hydrocarbon measurement use gas chromatography with either mass spectrometry or flame ionization detection. The use of proton transfer reaction mass spectrometry (PTR-MS) is becoming more wide spread in atmospheric chemistry research. The GC-MS is useful because it can provide very detailed chemical composition of an air sample. However, the sample collection process and the subsequent analysis by gas chromatography requires a considerable length of time so this method cannot be used for real time monitoring. The PTR-MS was developed in order to monitor pptv (parts per trillion volume) levels of VOCs in a short period of time without complex sample

preparations (19). The PTR-MS provides a less detailed chemical composition of a sample because it cannot distinguish between compounds of the same nominal mass but it does have some advantages. One advantage is the PTR-MS measures important oxygenated compounds such as formaldehyde and acetaldehyde that are difficult to sample and measure by gas chromatography. These compounds are directly emitted in exhaust and are created in photochemical reactions with VOCs in the atmosphere (20). Both are responsible for health problems (21) and are considered by the EPA as air toxics. The in-situ, high time resolution measurements of the PTR-MS can also be advantageous when there is a need to follow rapid changes in concentrations in ambient air or in laboratory experiments such as the engine exhaust tests described in Chapter 4.

In studies of urban air pollution, compounds from vehicle exhaust are ubiquitous and often the most abundant organic compounds in urban air. Urban air can often look like dilute vehicle exhaust with additional compounds from other sources such as solvent use and biogenic emissions. Mohamed et al.(22) found that in urban locations benzene, toluene, and the xylenes and ethylbenzene compounds (aromatics) were the most abundant organic species and correlated with vehicle emissions. Formaldehyde and acetaldehyde were also abundant. Organic gaseous compounds emitted in gasoline engine exhaust are alkenes, aromatics, and alkanes with 10 or fewer carbon atoms. The most abundant hydrocarbons are the n-alkanes (n-butane, n-pentane, n-hexane); the branched alkanes (isopentane, 2-methylpentane, 2,2,4-trimethylpentane); the unsaturated compounds (ethene, propene, ethyne); and the monoaromatics (benzene, toluene, p-xylene and m-xylene) (12, 23–25). Emissions of oxygenated organics such as formaldehyde and acetaldehyde are also significant (12). The gaseous phase of

diesel engine exhaust has not been as extensively characterized as gasoline exhaust but contains similar compounds to gasoline engine exhaust (23, 24, 26–28). One important difference is the much larger emission rate of formaldehyde and acetaldehyde from diesel engines, and emission of larger molecular weight compounds (26). The emission of larger molecular weight compounds reflects the very different fuel composition: gasoline consists of C₄ to C₁₀ hydrocarbons, while diesel is composed of C₆ to C₂₅ hydrocarbons (25–27, 29). It has been shown that the loading of the engine also affects the composition of the emissions, especially the abundance of alkenes and alkanes (30).

1.3 Partitioning hypothesis

In exhaust exposure chamber studies of health effects, animal subjects are submitted to a much higher concentration of organic particles than typically found in ambient air in order to obtain visible effects in a short period of time. However, these methods may affect the air chemistry. Organic compounds and semi volatile organic compounds like polyaromatic hydrocarbons (PAHs) can partition between the gas phase and the particulate phase. The partitioning of a compound between the gas and particulate phase is given by equation 1.1 from (18):

$$\frac{C_{aer}}{C_g} = K \times M_{taer} \quad (1.1)$$

where C_{aer} is the aerosol phase concentration ($\mu\text{g m}^{-3}$), C_g is the gas phase concentration ($\mu\text{g m}^{-3}$), M_{taer} is the total ambient aerosol mass concentration ($\mu\text{g m}^{-3}$), and K is the temperature-dependent coefficient characterizing the partitioning. Thus, the

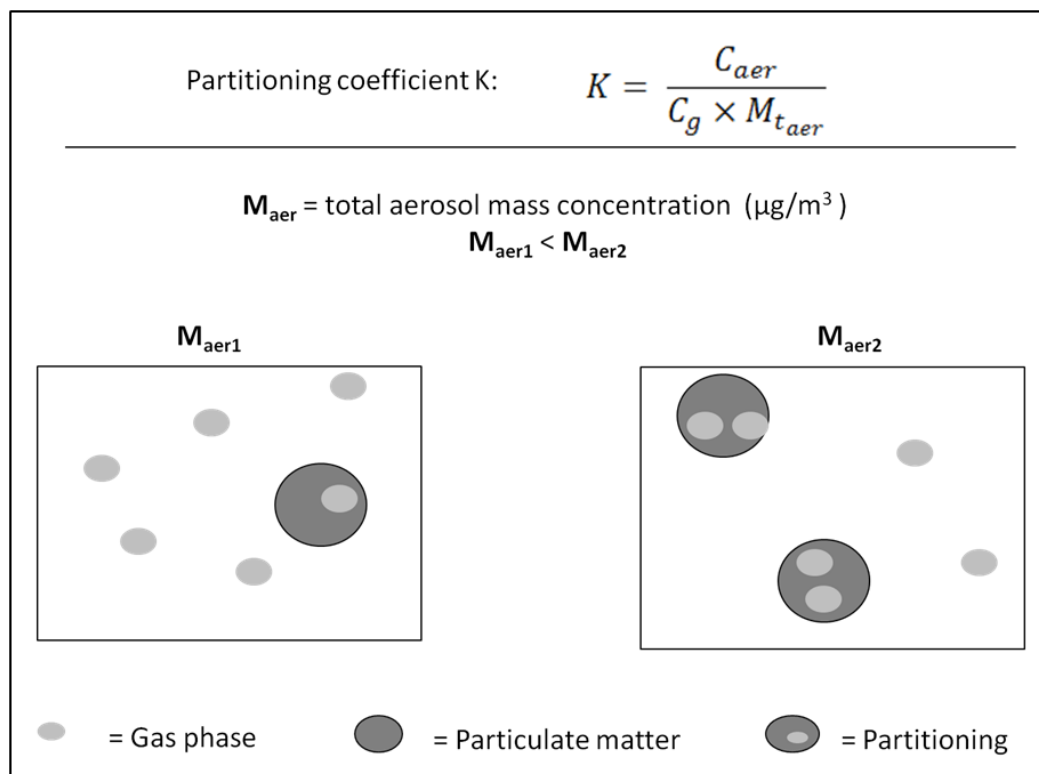


Figure 1.1. Illustration of the influence of the aerosol mass concentration in the partitioning process. An increase in the total aerosol mass concentration leads to the partitioning of the gas phase compounds into the particulate phase to maintain the equilibrium.

amount of organic compound that would condense into aerosol phase depends on the amount of organic aerosol present. A higher aerosol mass concentration would allow more partitioning from the gas phase to the condensed phase as illustrated in Figure 1.1. Exhaust exposure chambers are trying to mimic real world exposures to chemicals, but in scaling the exposure to high concentrations, the organic PM composition may be significantly different due to scavenging of compounds from the gas phase to the condensed phase. These particles then carry additional toxic chemical compounds to the lung.

Therefore, the effects of exhausts on health that have been observed with such high concentration chamber experiments may be misleading. The Lovelace Respiratory Research Institute has recently observed that gasoline and diesel exhaust mixtures have an even larger cardiovascular effect in mice than the sum of gasoline exhaust only and diesel exhaust only. The lipid peroxidal was used as the tracer to determine the health effect. High levels of lipid peroxides are associated with cancer and heart disease. A synergistic effect is observed; the sum of effects from pure exhaust is less than the effect for mixtures. Exhaust mixtures are important because this is what people are exposed to in the real world. As shown in Figure 1.2, a larger response results when the gasoline and diesel exhausts are mixed than the sum of the gasoline and diesel exhaust results separately. The mix of the two exhausts leads to more than three times the value expected. It is not clear why such a synergistic effect would occur. The working hypothesis illustrated in Figure 1.3 is that under the high particulate loadings used in the animal exposure tests ($300 \mu\text{g m}^{-3}$ or greater) the re-partitioning of gasoline exhaust compounds from the gas phase onto diesel particulate matter may increase the toxicity of inhalable particles. To better understand the relevance of the exposure chambers to real world conditions, measurements of gas phase organics by PTR-MS and particle phase composition by High Resolution Time-of-Flight Aerosol Mass Spectrometer (HR-ToF-AMS) were conducted as a multi-investigator study involving the Jobson and VanReken research groups from the Laboratory for Atmospheric Research at Washington State University (WSU), investigators from the School of Public Health at University of Washington, and the inhalation toxicology group from the Lovelace Respiratory Research Institute (LRRI) in Albuquerque, New Mexico. This thesis describes laboratory experiments to calibrate the PTR-MS in-

strument response to organic compounds expected to be in gasoline and diesel engine exhaust, and describes results from the exposure chamber characterization studies conducted at LRRI in the spring of 2012.

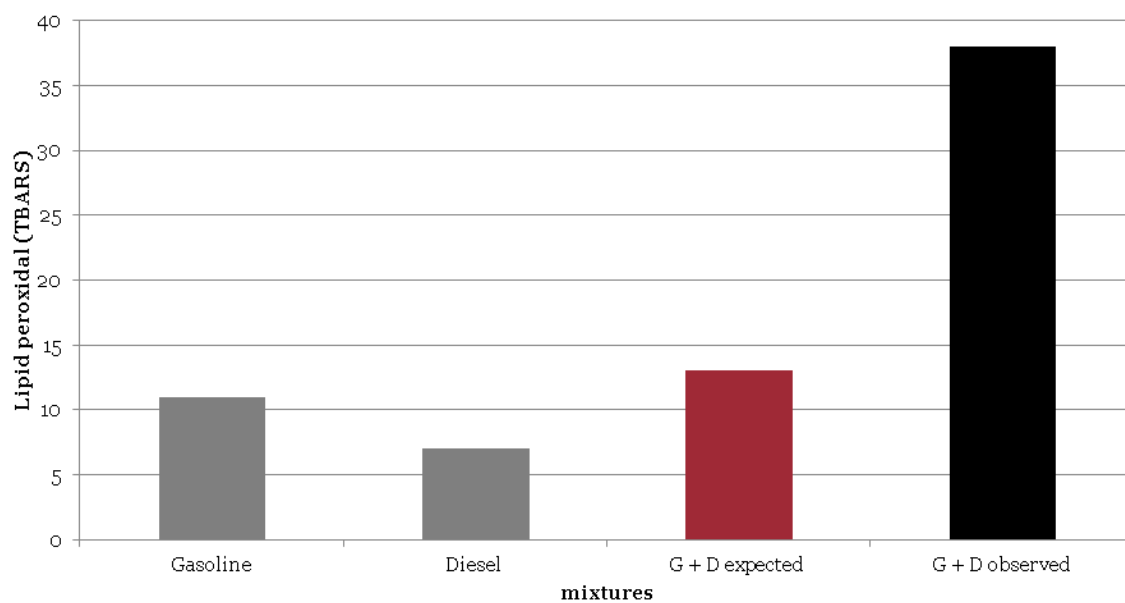


Figure 1.2. Lipid Peroxidal Response to Different Mixing Exposure (Source: LRRI results)

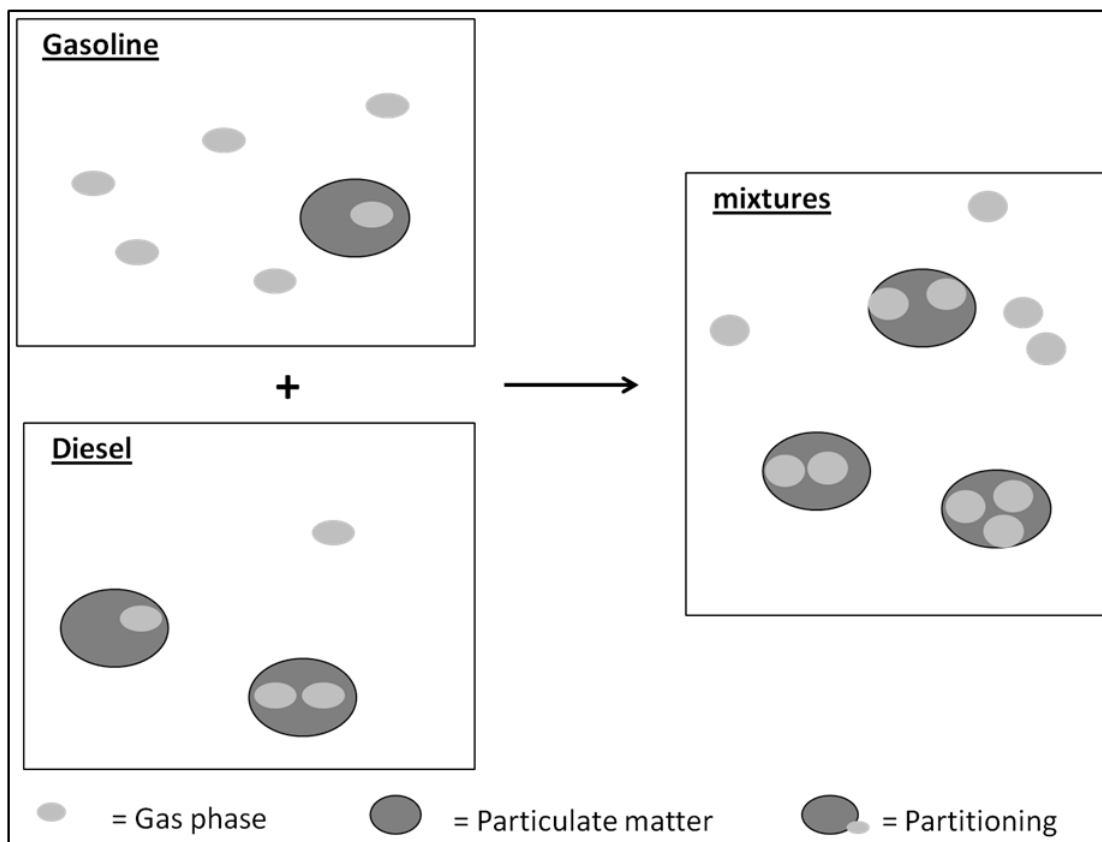


Figure 1.3. Illustration of the repartitioning hypothesis in mixtures of diesel and gasoline exhausts.

CHAPTER 2. EXPERIMENTAL SETUP

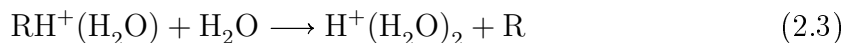
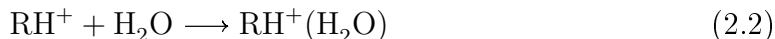
2.1 PTR-MS

2.1.1 PTR-MS measurement principle

The VOC measurements by the PTR-MS are based on a soft ionization of the organic compounds with the hydronium ion H_3O^+ . The method has been well described in literature (31), and only the basics of measurement are described in this section. The instrument is composed of an ion source, a drift tube, a quadrupole mass spectrometer and an ion detector as shown in Figure 2.1. The ion source produces a high density of hydronium ions from water vapor using a hollow cathode discharge. O_2^+ and NO^+ can also be produced but are considered as impurities. Those primary ions are transported into the drift tube reactor where the sample air is also introduced. The H_3O^+ ion does not react with gaseous components that have a proton affinity less than water vapor ($697 \pm 8 \text{ kJ mol}^{-1}$). As the major components of air have low proton affinity it acts like a buffer gas, and the organic compounds (R) with large enough proton affinities that are present in the sampled air undergo a non dissociative proton transfer reaction as described in equation 2.1:



where R is the organic compound present in the sample, H_3O^+ is the hydronium ion produced in the ion source and RH^+ is the product ion. O_2^+ and NO^+ can react with organic compounds which would interfere with the results so their concentrations in the drift tube are kept under 2% and 0.2% of H_3O^+ respectively. The drift tube is made of stainless steel rings separated by Teflon rings to isolate them electrically and connected by a resistor chain to create an electric field. This electric field enhances the kinetic energy of the ions so that collisions with the bath gas (air) cause desolvation of hydrated ions. The water vapor present in the drift tube can bind with the reagent ions H_3O^+ and the product ions RH^+ to form water clusters $\text{H}_3\text{O}^+(\text{H}_2\text{O})_n$ and $\text{RH}^+(\text{H}_2\text{O})_n$ where n is an integer. An interesting reaction that is of importance when sampling high VOC concentrations is that the $\text{RH}^+(\text{H}_2\text{O})$ water clusters can then react with H_2O and reform the R as described in following reactions 2.2, 2.3 called the Ligand switching reaction:



The extent of water cluster formation is a strong function of the drift tube pressure and electric field. To prevent the clustering and thus simplify the mass spectrum, the reaction chemistry is performed in a drift tube so the clusters concentrations are reduced to a minimum by collision induced dissociation with air molecules in the drift tube. Drift tube reaction dynamics are characterized by the ratio of the electric field E (volts per centimeter) over the number density of gas N (cm^{-3}) in the drift

tube according to equation 2.4. The units of this ratio are expressed in Townsend (Td) where 1 Td is equal to 10^{-17} (V cm^{-2}).

$$\text{Drift field strength} = \frac{E}{N} \quad (\text{V cm}^{-2}) \quad (2.4)$$

The number density of air in the drift tube is temperature and pressure dependent. An increase in the electric field (higher Td) results in more energetic collisions and less clustering but also leads to a greater degree of dissociative protonation and the creation of organic fragment ions. Such fragmentation is not desirable since the interpretation of the PTR-MS mass spectrum relies upon its presentation as a simple M+1 mass spectrum where M is the molecular weight of R. The instrument is usually run at 120-150 Td with the drift tube pressure at 2 mbar. Ions are sampled from the drift tube by electrostatic lenses and are mass filtered by a quadrupole mass spectrometer. Ions are detected and counted with a secondary electron multiplier detector (SEM). The H_3O^+ ion count rate is typically 5 MHz and is much higher than the concentration of the product ions RH^+ so that the concentration of R can be calculated as given in equation 2.5:

$$[R_i] = \frac{[\text{RH}^+]}{k_i \cdot t \cdot [\text{H}_3\text{O}^+]} \times \frac{\varepsilon_{[\text{RH}^+]}}{\varepsilon_{[\text{H}_3\text{O}^+]}} \quad (2.5)$$

where $[R_i]$ is the number density of the organic compound i, $[\text{RH}^+]$ is the measured count rate of the product ion (Hz), $[\text{H}_3\text{O}^+]$ is the measured count rate of the reagent ion (Hz), t is the reaction time that corresponds to the time H_3O^+ spent in the drift tube (about 0.1ms), k_i is the H_3O^+ reaction rate constant with compound i, and $\varepsilon_{[\text{RH}^+]}$ and $\varepsilon_{[\text{H}_3\text{O}^+]}$ are the ion transmission efficiencies through the quadrupole

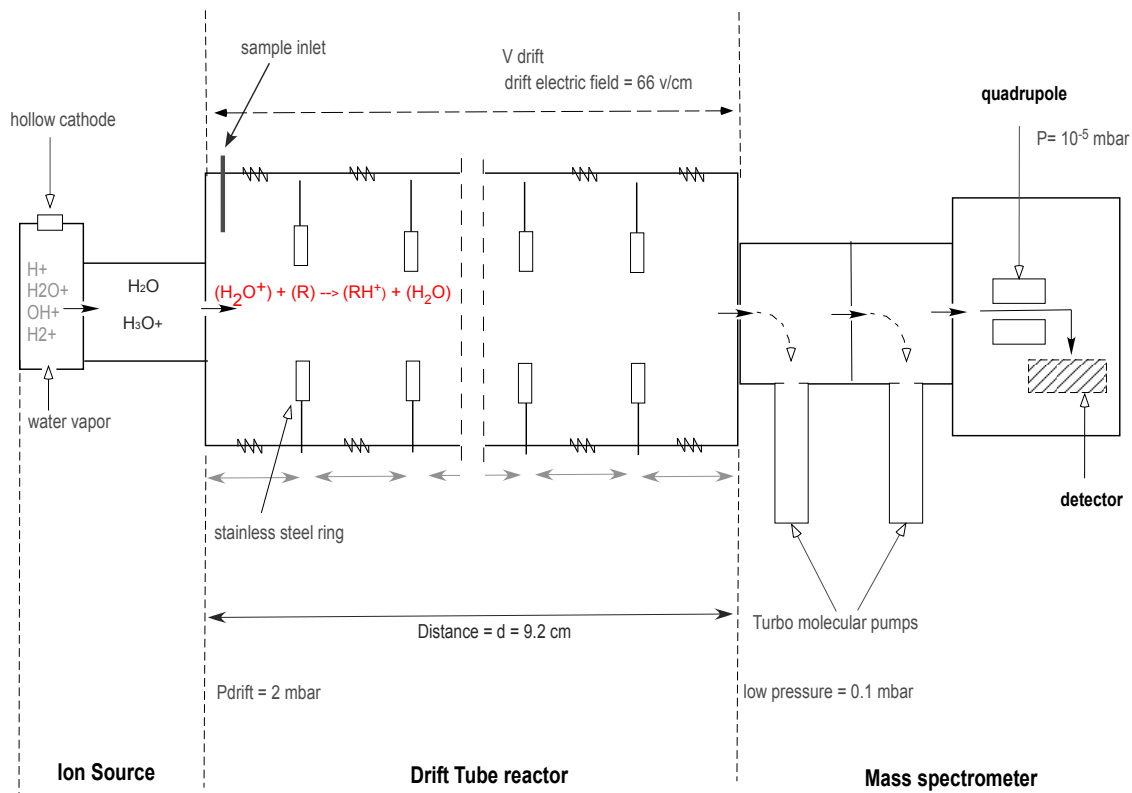


Figure 2.1. Schematic of the PTR-MS

for RH^+ and H_3O^+ respectively. The PTR-MS measurements result in mass spectra (m/z) of the protonated compounds (molecular weight of $MW+1$ that were detected by the quadrupole. The mass spectrometer is operated in either a scan mode whereby all ions over some m/z range are consecutively measured or in MID mode whereby only selected ions are measured. An example of a mass spectrum obtained from a calibration tank experiment is shown in Figure 2.2.

The VOC analysis can be improved by using a water trap that removes the water vapor from a sample to reduce clustering and allows the drift tube to be operated at lower Townsend numbers (32). The advantage of operating the PTR-MS at lower

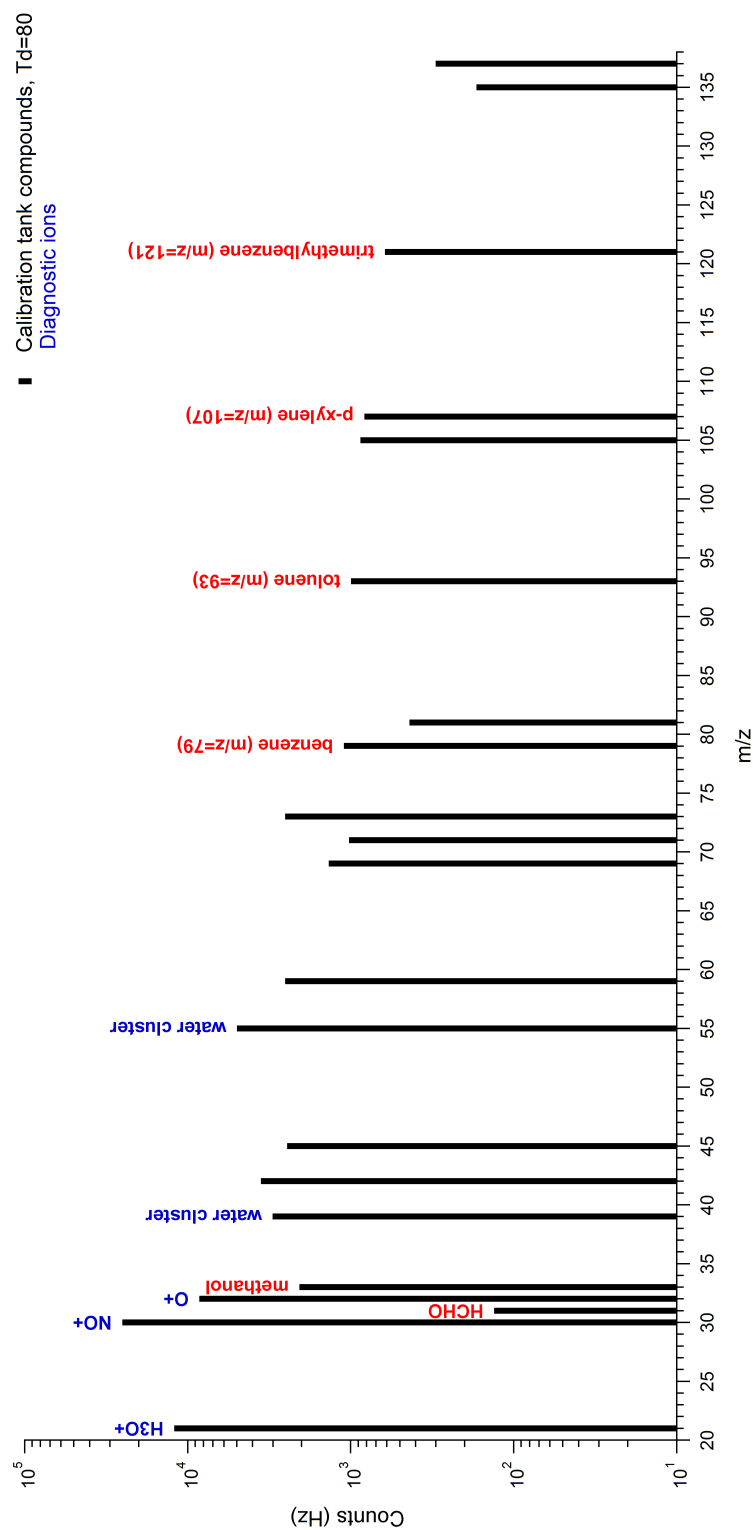


Figure 2.2. PTR-MS mass spectrum of a calibration tank experiment at Td80

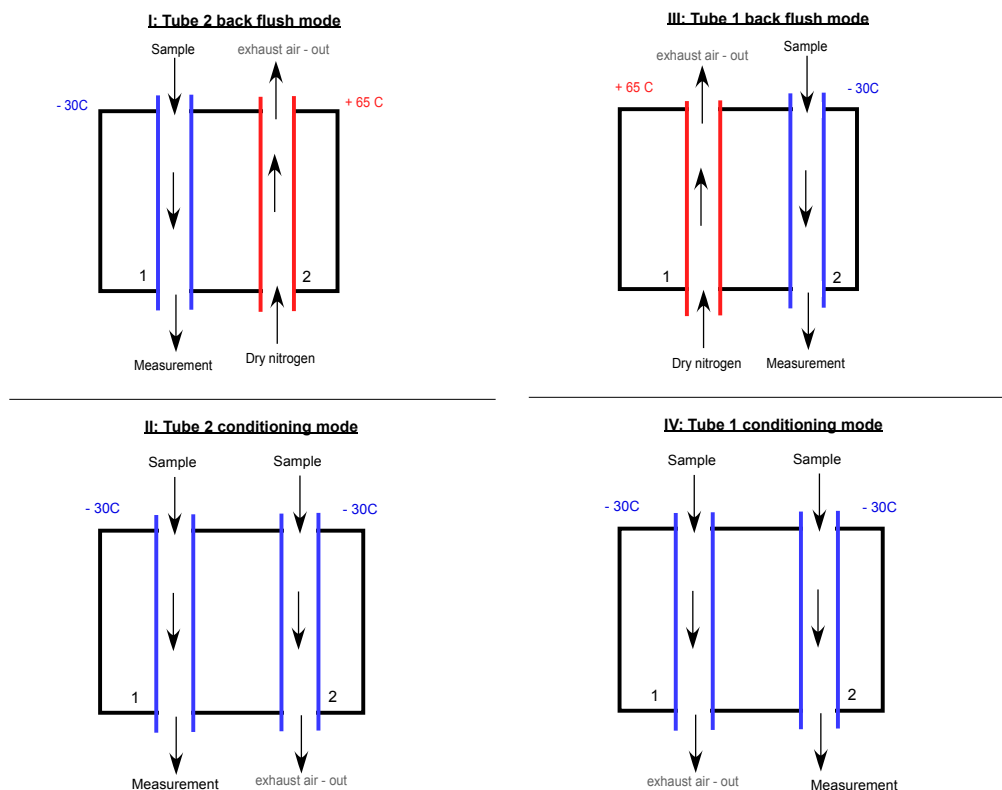


Figure 2.3. Four modes of the cold trap. The tubes are measuring one after the other. For each tube there are three periods of time: a back flush period to eliminate any compounds from the previous measurement with a temperature of 65°C, a conditioning period characterized by a cold temperature of -30°C, and a measurement period when the PTR-MS samples air flowing through the tube.

Td values, such as 80Td, is increased sensitivity, reduced fragmentation, and a vast improvement in the measurement of formaldehyde which displays a water vapor dependent sensitivity. The cold trap is composed of two tubes that are run in four modes as describes in Figure 2.3. The PTR-MS used in this work is operated with a water trap. To measure volatile organic compounds the sample is dried by passing the air through a cold trap held at -30°C. Furthermore, a second inlet has been added to improve detection limits of higher molecular weight compounds that are present at low concentrations.

2.1.2 Intermediate volatile organic compounds (IVOCs) measurements

The IVOC species are present at lower concentrations, so are difficult to measure directly by PTR-MS. The thermal desorption system that has been developed accumulates the sampled air on a Tenax TA adsorbent resin to obtain higher concentrations of IVOCs that are measurable by the PTR-MS. Sampling through the Tenax eliminates the compounds with higher volatility from the sample air so that it is possible to distinguish between volatile compounds and higher molecular weight organics by using the combination of the water trap and the thermal desorption system. The VOC and the IVOC inlets are separate but instrument operation allows for switching from one inlet to the other as shown in Figure 2.4. The IVOC system runs by cycles of four consecutive modes: sample mode, purge mode, measure mode and back flush mode. Each is characterized by a specific Tenax trap temperature and a time period. The measurements of VOCs are implemented while the sample is being collected on the Tenax trap. The sample mode corresponds to the collection of the sample on the Tenax tube for usually 180 seconds at 30°C. The compounds with lower volatility are more efficiently adsorbed than those with high volatility. The purge mode consists in flowing dry nitrogen through the Tenax to flush out the lighter compounds. A longer purge time at a higher temperature would remove more compounds. The typical purge time period is about 120 seconds at 150°C. During the measure mode the air flow is pushed through the Tenax in the opposite direction to the drift tube. For the IVOC measurements time is limited, therefore we need to choose the specific masses that we want to work on before running the experiment, to have enough time and obtain a good data set. Usually the measurement period lasts for 300 seconds at a 230°C. The fourth mode, back flush, is used to clean up the Tenax. The temperature

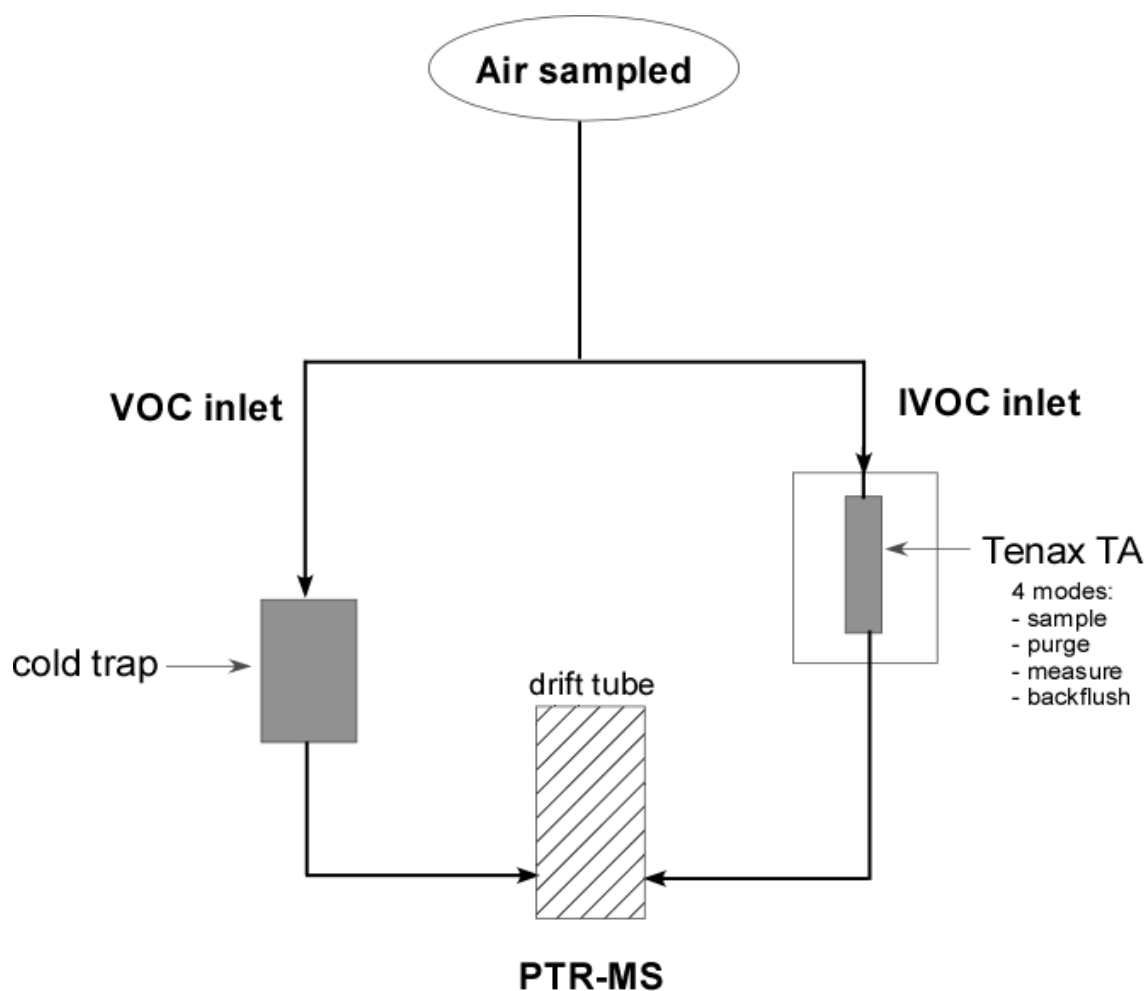


Figure 2.4. Schematic of the VOC/IVOC system

and the time period are usually 230°C for 180 seconds, and the air flow is directed the opposite way as the measure mode to remove compounds still in the trap so it is clean for the next cycle.

2.2 Dynamic Dilution System

A dynamic dilution system based on a syringe pump to dispense accurate molar flows of liquid chemical compounds was used to prepare test mixtures for analysis by PTR-MS. A recent study from C.L. Faiola et al. (33) showed good results from this system that was used to generate standard mixtures of trace VOCs. Here, the dynamic dilution system was used to make test mixtures of compounds that are not stable as compressed gas mixtures. These test mixtures were used to examine fragmentation patterns and to determine the sensitivity of the PTR-MS to PAH compounds. The accuracy of the dynamic dilution systems was evaluated by comparing test mixtures prepared from neat liquids against the compressed gas VOC standard typically used to calibrate the PTR-MS. The experimental set-up of the dynamic dilution system was similar for both types of tests with a few exceptions as described below.

2.2.1 Injection of test mixtures

The dynamic dilution system is divided into three parts for ease of description: the dry nitrogen dilution flow, the syringe pump, and the test mixture flow. The set-up of the dilution system is sketched in Figure 2.5. A known molar flow rate of a compound is injected using the syringe pump into a heated zone where it evaporates from the syringe tip and is diluted by a dry nitrogen flow supplied from a liquid nitrogen dewar. The PTR-MS subsampled from the test mixture flow and the rest of the flow was vented to the laboratory fumehood. The dry nitrogen flow was controlled by a MKS mass flow controller to provide a known dilution flow. The syringe pump used was a Harvard Apparatus PHD 2000 infusion pump. The syringe type used in the

experiments was the Hamilton Gastight in a size range of 0.1 to 50 μl . The tubing and fittings for the system were stainless steel or Restek Sulfinert coated stainless steel tubing. To keep the injected compounds in the gas phase and avoid potential wall losses, the tubing and fittings were heated using heat tape. The temperature of the injection zone (T_1) was thermostated using a temperature controller (Watlow) with a type K thermocouple wire measuring the airflow temperature at point T_1 as shown in the Figure 2.5. Typical injection temperatures were between 30 and 70°C. A second thermocouple measured the temperatures immediately downstream of the injection zone (T_2). The stainless steel tubing downstream from the injection zone was coiled to enhance mixing. This tubing was wrapped in heat tape and the temperature controlled by a variac. Downstream tubing temperature was estimated to range between 80 and 90°C. This temperature may have influenced the actual temperature of the injection by heat conducted through the hot tubing. A difference in temperature between T_1 and T_2 was observed as shown in Figure 2.6. At T_1 set point temperatures of between 30 and 40°C, the difference between T_1 and T_2 is small, on the order of a few degrees. At a set-point temperature of 50°C, the downstream temperature at T_2 was about 10°C warmer. At a T_1 temperature of 70°C and greater the T_2 temperature was consistently about 90°C, and reflects the temperature of the downstream tubing temperature.

2.2.2 Calculations of test mixture molar mixing ratios

The molar mixing ratio of the prepared test mixture (X_i) can be calculated from the molar flow of the injected liquid (MF_i) and the molar flow of the diluting gas (MF_{N_2}) as given in equation 2.6 .

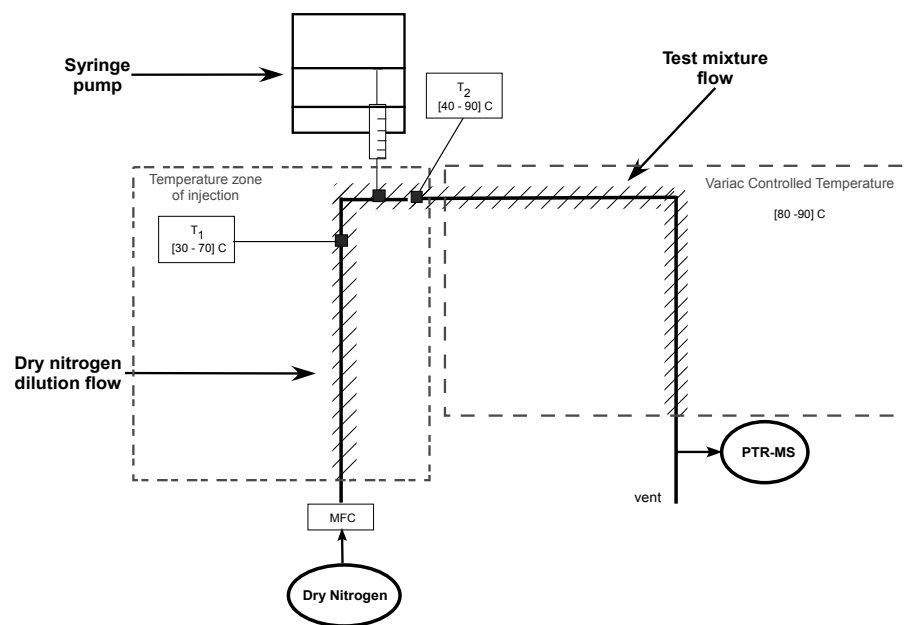


Figure 2.5. Diagram of the dynamic dilution system setup for making ppbv test gas mixtures from liquid chemicals.

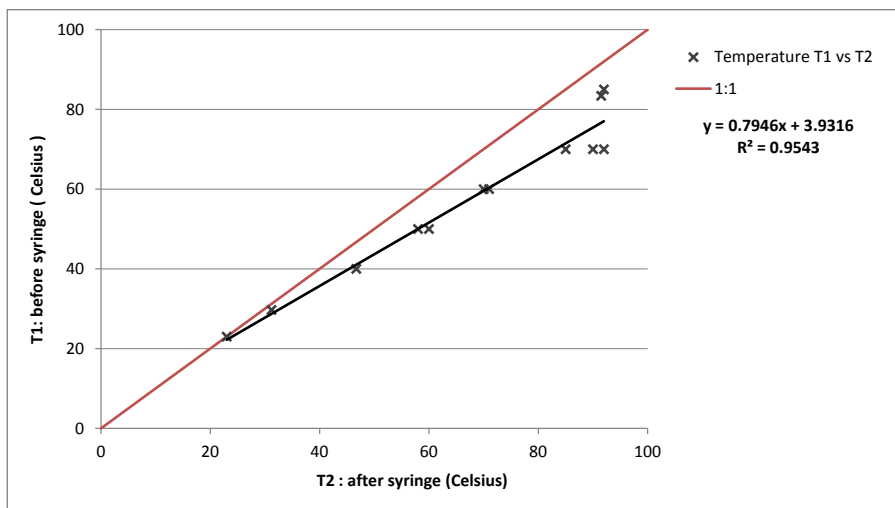


Figure 2.6. Temperature difference in the dynamic dilution system between T_1 and T_2

$$X_i = 10^9 \times \frac{MF_i}{MF_{N_2}} \quad (\text{ppbv}) \quad (2.6)$$

Those two molecular flows can be determined as shown in equation 2.7,

$$X_i = 10^9 \times \frac{I_r \times \frac{\mu_i}{1000 \times MW_i}}{60 \times \frac{GF_{N_2}}{V_{m_{N_2}}}} \quad (\text{ppbv}) \quad (2.7)$$

where I_r is the infusion rate of the syringe pump in $\mu\text{l hr}^{-1}$, μ_i is the density of the compound i in g mL^{-1} , MW_i is the molecular weight of the compound i in g mol^{-1} , GF_{N_2} is the gas flow of the dry nitrogen in slpm, and $V_{m_{N_2}}$ is the molar volume of gas at standard temperature and pressure. The standard temperature and pressure reference conditions used by the MKS mass flow controller are 1 atmosphere and 273 K, resulting in a molar volume of 22.42 L mol^{-1} . Some of the compounds examined (acenaphthene, biphenyl and acenaphthylene) were in the solid phase at room temperature. For a solid compound j , it was necessary to first dissolve it in a solvent. C_j is the concentration resulting from that dissolution. Dichloromethane was chosen as a solvent for the dissolution because it has a proton affinity lower than H_2O and therefore can't be detected by the PTR-MS. The molar flow of the solid compound j injected by the syringe pump does not depend on the density anymore but on the solution concentration C_j . The test mixture molar mixing ratio is given by 2.8:

$$X_j = 10^9 \times \frac{I_r \times \frac{C_j}{1000 \times MW_j}}{60 \times \frac{GF_{N_2}}{V_{m_{N_2}}}} \quad (\text{ppbv}) \quad (2.8)$$

where C_j is the concentration of the compound j in g mL^{-1} . Solutions were made up

using 10 mL and 100 mL volumetric flasks. The solid compounds were weighed using an analytical balance (Mettler H₂O WWR scientific) that allows a precision to 10⁻⁵ g. The final C_j was about 0.002 g mol⁻¹.

2.2.3 PTR-MS calibration with a compressed gas standard

To determine the accuracy of the dynamic dilution system the setup is slightly different because we are mixing two gas flows, the one from the compressed gas multi-component calibration tank and the other from the dilution flow of dry nitrogen. The set up for the calibration study is described in Figure 2.7. The set up is divided into three parts again for ease of description: the dry nitrogen dilution flow, the calibration tank flow, and the test mixture flow connected to the PTR-MS inlet. The calibration for the PTR-MS is performed using a special tank composed of known concentrations of specific VOCs. The tank used in our laboratory is from Scott Marrin, Inc, and its whole composition is detailed in Table 2.1. The accuracy of the standard is $\pm 10\%$ as stated by the manufacturer. The sensitivities of the PTR-MS for those compounds can be calculated using equation 2.9 :

$$S_i = \frac{NC}{X_i} \quad (\text{Hz per MHzH}_3\text{O}^+ \text{ per ppbV}) \quad (2.9)$$

$$X_i = \frac{C_i \times F_c}{F_d + F_c} \quad (\text{ppbv}) \quad (2.10)$$

where S_i is the sensitivity of the compound i, NC is the normalized count from the PTR-MS measurement (Hz per MHzH₃O⁺ per ppbV), X_i the compounds molar mixing ratio in ppbv calculated from equation 2.10, C_i is the mixing ratio of compound

i in the calibration tank in ppbv, F_c is the flow from the calibration tank in sccm (typically 10 sccm), and F_d is the dilution flow of dry nitrogen in sccm (typically 1016 sccm).

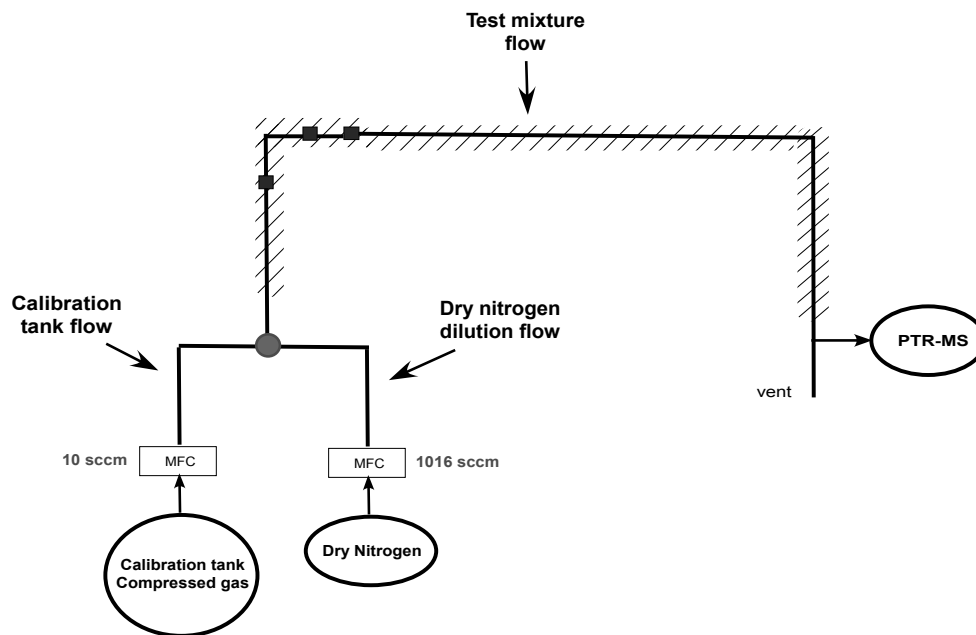


Figure 2.7. Diagram of the dynamic dilution system setup for calibration tests using a compressed gas standard.

Table 2.1. Mixing Ratios of VOCs in the PTR-MS Calibration Standard tank

No.	Compound	MW (g·mol ⁻¹)	m/z	Mixing ratio (ppmv)
1	methanol	32	33	2
2	acetonitrile	41	42	2
3	acetaldehyde	44	45	2
4	acetone	58	59	2
5	isoprene	68	69	2
6	methacrolein	70	71	2
7	2-butanone (MEK)	72	73	2
8	benzene	78	79	2
9	toluene	92	93	2
10	styrene	104	105	2
11	p-xylene	106	107	2
12	1,2,4-trimethylbenzene	120	121	2
13	a-pinene	136	137	2
14	1,2,3,5-tetramethylbenzene	134	135	0.5

CHAPTER 3. EXPERIMENTAL RESULTS

3.1 Dynamic Dilution System

3.1.1 Accuracy of the syringe pump infusion rate

The volume of the compounds injected into the dynamic dilution system is in the order of μL , thus the accuracy of the syringe pump was verified. Two syringes S_1 and S_2 of $50 \mu\text{L}$ were filled with p-xylene and weighed using the analytical balance before and after injection. The expected volume loss was calculated from the infusion rate and the time of infusion as shown in equation 3.1. The expected mass loss was calculated with the density of p-xylene as shown in equation 3.2 :

$$\text{Expected volume loss} = I_R \times T \quad (3.1)$$

where I_R is the infusion rate in $\mu\text{l hr}^{-1}$ and T is the time of infusion in hr.

$$\text{Expected mass loss} = \text{Expected volume loss} \times \mu \quad (3.2)$$

where μ is the density of p-xylene $8.61 \cdot 10^{-4} \text{ g } \mu\text{l}^{-1}$

Four tests were performed and the results are summarized in Table 3.1. The average

volume error between the expected and actual loss was $0.5\% \pm 1$. The small mass loss was more difficult to measure and the results present larger average mass error loss of $-0.7\% \pm 8.3$. The negative value is representative of a smaller measured mass loss than the expected one. According to those results, the syringe pump is considered accurate for further analysis.

Table 3.1. Results on the accuracy of the syringe pump infusion rate

	units	test 1 (S1)	test 2 (S2)	test 3 (S2)	test 4 (S2)
volume initial	ul	50	50	50	50
volume final	ul	0	37.5	37.5	41.5
volume loss	ul	50	12.5	12.5	8.5
mass initial	g	24.536	24.349	24.343	24.342
mass final	g	24.495	24.339	24.331	24.335
mass loss	g	0.041	0.010	0.012	0.007
Infusion rate	ul hr	50	50	50	50
time	hr	1	0.25	0.25	0.1667
expected volume loss	ul	50.0	12.5	12.5	8.3
expected mass loss	g	0.043	0.011	0.011	0.007
volume difference	%	0%	0%	0%	2%
mass difference	%	-5%	-7%	11%	-2%

3.1.2 Aromatic Sensitivities

Sensitivity tests for compounds present in the compressed gas calibration tank have been performed and their final average sensitivities at Td=80 and Td=120 are given in Table 3.2. The calibration tank flow remained open for at least 3 hours and sometimes overnight (but less than 24 hours) to condition all tubing before measurements were made. The concentration of the compounds present in the calibration

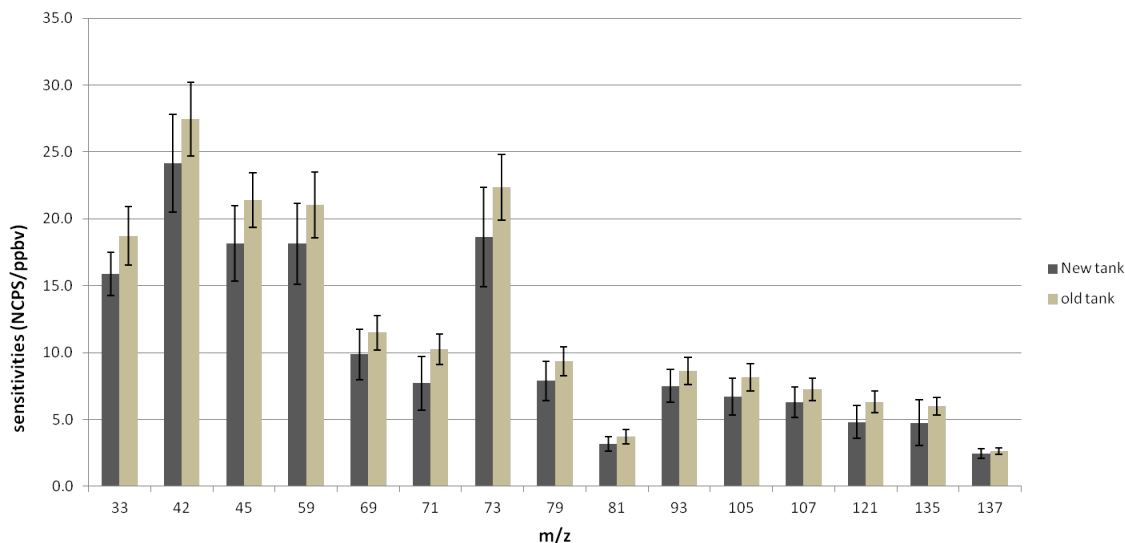


Figure 3.1. Comparison of the averaged sensitivities between the new tank and old tank.

tanks were confirmed by analysis on a GC-MS system. Two identical VOC calibration tanks from Scott Marrin were compared, one older and nearly depleted and the other newer. Results in Figure 3.1 shows the resulting normalized sensitivities and these were generally within the 10% expected accuracy. The old tank sensitivity values are slightly higher. To determine the importance of conditioning another experiment was performed whereby the cal gas flowed for 5 days instead of less than 24h. The sensitivities were higher and the results are shown in Table 3.2. According to those tests the sensitivity values are influenced by the conditioning time, requiring more than 24 hours.

Table 3.2. Final aromatic sensitivities (NCPS) at Td80 and Td120 for a conditioning time of less than 24h and more than 5 days. Percent difference for the two conditioning time results.

conditioning time: $\leq 24h$			conditioning time: $\geq 5days$			% difference
m/z	Sensitivity Td80	Sensitivity Td120	m/z	Sensitivity Td80	Sensitivity Td120	
33	15.9 \pm 1.6	9.6 \pm 1.0	33	21.2	10.4	25%
42	24.2 \pm 3.7	14.3 \pm 1.3	42	34.7	19.3	30%
45	18.2 \pm 2.8	11.2 \pm 1.4	45	49.6	18.2	63%
59	18.1 \pm 3.0	10.8 \pm 1.5	59	26.7	14.8	32%
69	9.9 \pm 1.9	5.3 \pm 1.0	69	14.5	6.9	32%
71	7.7 \pm 2.0	4.3 \pm 1.0	71	11.4	5.0	32%
73	18.7 \pm 3.7	10.8 \pm 2.0	73	27.4	15.3	32%
79	7.9 \pm 1.5	5.1 \pm 1.0	79	12.1	7.9	35%
81	3.2 \pm 0.5	2.5 \pm 0.5	81	4.9	4.0	35%
93	7.5 \pm 1.2	4.7 \pm 0.9	93	11.0	6.9	31%
105	6.7 \pm 1.4	4.1 \pm 1.0	105	9.9	6.3	32%
107	6.3 \pm 1.1	3.8 \pm 0.8	107	9.0	5.6	30%
121	4.8 \pm 1.2	3.0 \pm 0.8	121	6.8	4.1	29%
135	4.8 \pm 1.7	2.1 \pm 1.3	135	7.3	4.3	35%
137	2.4 \pm 0.4	1.1 \pm 0.2	137	3.1	1.5	22%

3.1.3 Accuracy of the dynamic dilution system

Mixtures of 4 compounds, benzene, toluene, p-xylene and 1,3,5-trimethylbenzene were prepared to test the accuracy of the dynamic dilution system. Those compounds were present in the Scott Marrin calibration standard and their sensitivities were already determined (see Table 3.2). The tests were usually run at 5 injection manifold temperatures: $T_1=30^{\circ}\text{C}$, $T_1=40^{\circ}\text{C}$, $T_1=50^{\circ}\text{C}$, $T_1=60^{\circ}\text{C}$, $T_1=70^{\circ}\text{C}$. Benzene was also run at room temperature. The infusion rates were varied between $0.1\ \mu\text{l hr}^{-1}$, $0.25\ \mu\text{l hr}^{-1}$, $0.5\ \mu\text{l hr}^{-1}$, and $5\ \mu\text{l hr}^{-1}$ with a nitrogen flow of 15 slpm or 20 slpm. At $0.1\ \mu\text{l hr}^{-1}$ no test for benzene and pxylene were run. The ranges of the expected concentrations for the 4 compounds are given in Table 3.3. The tests were divided into two sets: low mixing ratio tests that correspond to mixing ratios ≤ 200 ppbv and high mixing ratio tests that correspond to mixing ratios ≥ 800 ppbv.

Table 3.3. Ranges of expected mixing ratio for benzene, toluene, p-xylene and 1,3,5-trimethylbenzene.

Compounds	Mixing ratio range (ppbv)				
	low mixing ratios				high mixing ratio
<i>Infusion rate (ul/hr)</i>	<i>0.1</i>	<i>0.25</i>	<i>0.5</i>	<i>0.1</i>	<i>5</i>
<i>N2 Flow (slpm)</i>	<i>15</i>	<i>15</i>	<i>15</i>	<i>20</i>	<i>20</i>
benzene	28	70	140	.	1350
toluene	23	58	116	17	1126
pxylene	20	50	109	.	973
1,3,5-trimethylbenze	18	45	91	14	875

The 1,3,5-trimethylbenzene is the less volatile compound tested with the lower vapor pressure. This compound displays a good correlation between the expected and measured mixing ratios as shown in Figure 3.2. The measured mixing ratios are

within the 20% of the expected mixing ratios. At smaller infusion rates the measured mixing ratio is higher than expected, and for the expected 875 ppbv test mixture the measured mixing ratio is smaller by less than 10%. The $T=40^{\circ}\text{C}$ results for low mixing ratios and the two data points for $T=50^{\circ}\text{C}$ come from the same experiment that is considered as an outlier for the analysis because the points do not follow the trend of all the other points. The error bars correspond to the standard deviation of multiple tests.

The p-xylene also displays a good correlation between the expected and measured mixing ratios as shown in Figure 3.3. The measured mixing ratios are smaller than expected by less than 20% for mixing ratios less than 120 ppbv at $T=30^{\circ}\text{C}$ to $T=70^{\circ}\text{C}$. For the expected mixing ratio of 973 ppbv, at $T=30^{\circ}\text{C}$, 40°C and 50°C the measured and expected mixing ratio match; at $T=60^{\circ}\text{C}$ and $T=70^{\circ}\text{C}$ the measured mixing ratios are larger by less than 10% and 20% respectively. The $T=40^{\circ}\text{C}$ results for low mixing ratios and the two data points for $T=50^{\circ}\text{C}$ are considered as outliers in this analysis as it comes from the same experiment previously described as an outlier for 1,3,5-trimethylbenzene. The error bars correspond to the standard deviation of multiple tests.

The results for toluene are shown in Figure 3.4. The measured concentration at $T=40^{\circ}\text{C}$ is within 20% of the expected concentration and within 30% of the highest infusion rate that produced a 1126 ppbv test mixture. At $T=50^{\circ}\text{C}$ there is good agreement between the expected and measured mixing ratios, within 20% for mixing ratios less than 60 ppbv. At $T=60^{\circ}\text{C}$, the results show that the measured mixing ratio is always higher than expected, at 18 ppbv expected the measured mixing ratio is less than 20% higher, but for the other expected concentration the measured mixing

ratios are more than 20% higher. At $T=70^{\circ}\text{C}$ the measured mixing ratios are higher than expected for both low (18 ppbv) and high (1126 ppbv) mixing ratios. At the 116 ppbv expected there is a point that shows a measured mixing ratio lower by more than 20% at $T=50^{\circ}\text{C}$ and a point in the 20% difference range at $T=60^{\circ}\text{C}$. Those two points result from the same experiment set and do not follow the trend of the other points perhaps due to incorrectly recorded flows, so both are considered as outliers. For a mixing ratio less than 120 ppbv the ideal temperature to run toluene is around $T=40^{\circ}\text{C}$, measured mixing ratios are lower than expected by more or less 20%. At small mixing ratios (low infusion rates) and low temperature the excessive evaporation appears to be an influence for toluene. At $T=60^{\circ}\text{C}$ and $T=70^{\circ}\text{C}$ the infusion rate may too low given the toluene vapor pressure at these temperatures and excessive evaporation from the syringe may be producing higher count rates than expected.

Benzene is the most volatile compound tested with the higher vapor pressure. All the mixing ratios measured are higher than expected for the whole temperature range as shown in Figure 3.5. For an expected mixing ratio of 28 ppbv, at T_{room} the measured mixing ratio is 10% larger. For an expected mixing ratio of 70 ppbv, the measured mixing ratio was larger by more than 20% at T_{room} , more than 30% at $T=40^{\circ}\text{C}$ and more than 40% at $T=50^{\circ}\text{C}$. For an expected mixing ratio of 140 ppbv, the measured mixing ratio at T_{room} , $T=40^{\circ}\text{C}$ and $T=50^{\circ}\text{C}$ are all larger by more than 30%. For the expected mixing ratio of 1340 ppbv, the measured concentration are less than 10% larger at $T=30^{\circ}\text{C}$ and $T=40^{\circ}\text{C}$, less than 20% larger at $T=50^{\circ}\text{C}$ and $T=60^{\circ}\text{C}$, and 30% larger at $T=70^{\circ}\text{C}$. The small expected concentrations were obtained with an infusion rate of $0.1\ \mu\text{l hr}^{-1}$, $0.25\ \mu\text{l hr}^{-1}$, and $0.5\ \mu\text{l hr}^{-1}$, and the high expected concentration was obtain for an infusion rate of $50\ \mu\text{l hr}^{-1}$. The results

show that only at higher infusion rates is the measured concentration close to what is expected, and the difference increases as the infusion manifold temperature increases. The discrepancy is likely due to benzene vapor diffusing from the syringe tip at a rate that is greater than the infusion rate. At higher infusion manifold temperatures and low infusion rates, this evaporative loss might be causing a greater mass loss of benzene than is calculated from the infusion rate and lead to higher measured mixing ratios. The usefulness of the dynamic dilution system may be limited to lower volatility compounds and higher infusion rates.

The test conditions are summarized in Figure 3.6. The figures show the vapor pressures of the aromatics tested versus temperature. The plain circles around data points indicate tests where the measured mixing ratio was within 20% of the expected mixing ratio. The data points with dashed circles indicate tests conditions where the measured mixing ratio was more than 20% greater than expected. In general, we can conclude that for infusion rates less than $0.5 \mu\text{l hr}^{-1}$ the best results (agreement within 20%) were obtained when compound vapor pressures were less than 100 Torr. For infusion rates of $50 \mu\text{l hr}^{-1}$, manifold temperature leading to vapor pressures up to 300 Torr could be used. For best operation of the dynamic dilution system it makes sense that the injection manifold temperature be adjusted to account for the compounds volatility. Operating at too high a temperature may cause excessive evaporation from the syringe and a mass loss that is greater than the infusion rate. If the injection manifold temperature is too low it was observed that an erratic PTR-MS signal would result suggesting droplet formation and loss from the syringe tip. The dynamic dilution system was put together to determine the sensitivities of the compounds like PAHs that are important for the characterization of the exhausts but

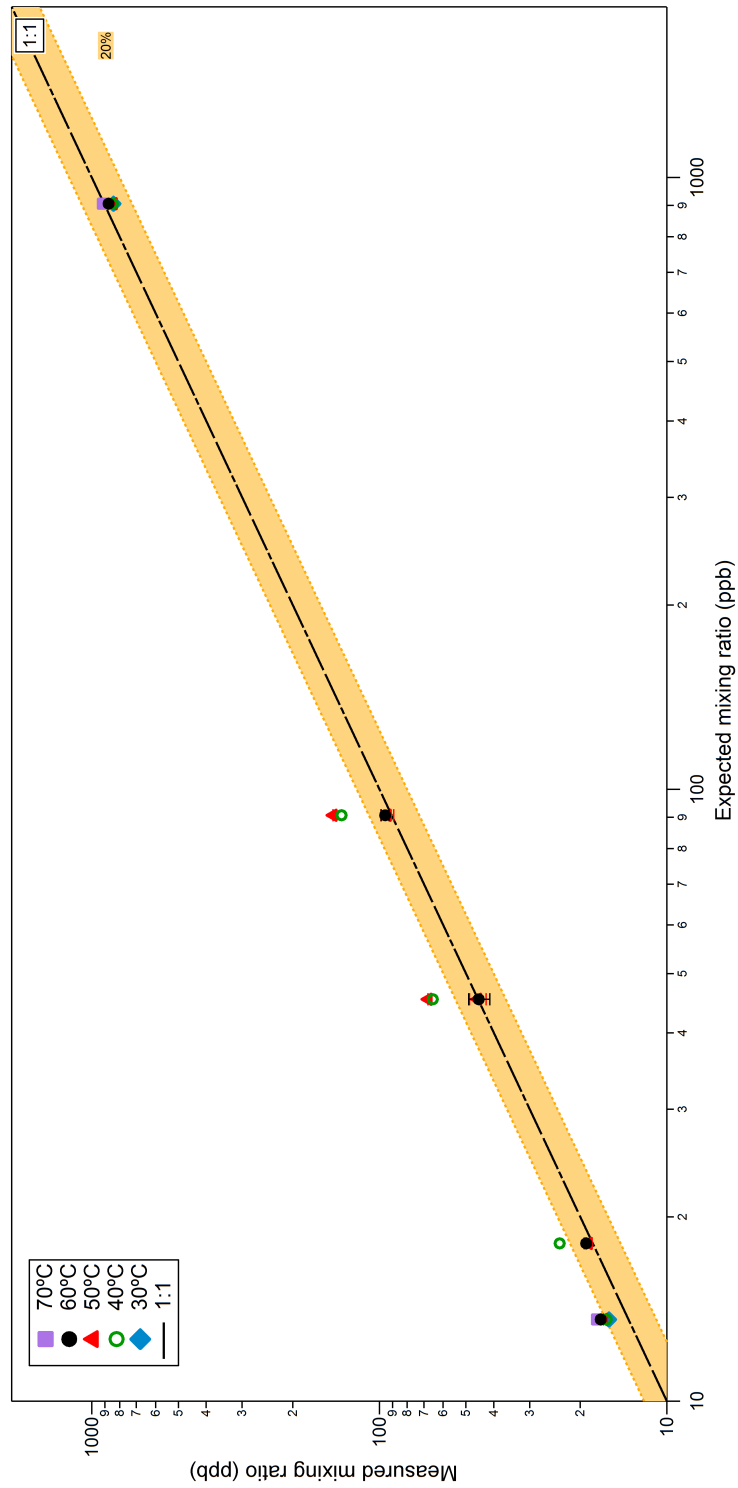


Figure 3.2. 1,3,5-trimethylbenzene: measured concentration against expected concentration for a temperature range of $[T=30^{\circ}\text{C} : T=70^{\circ}\text{C}]$

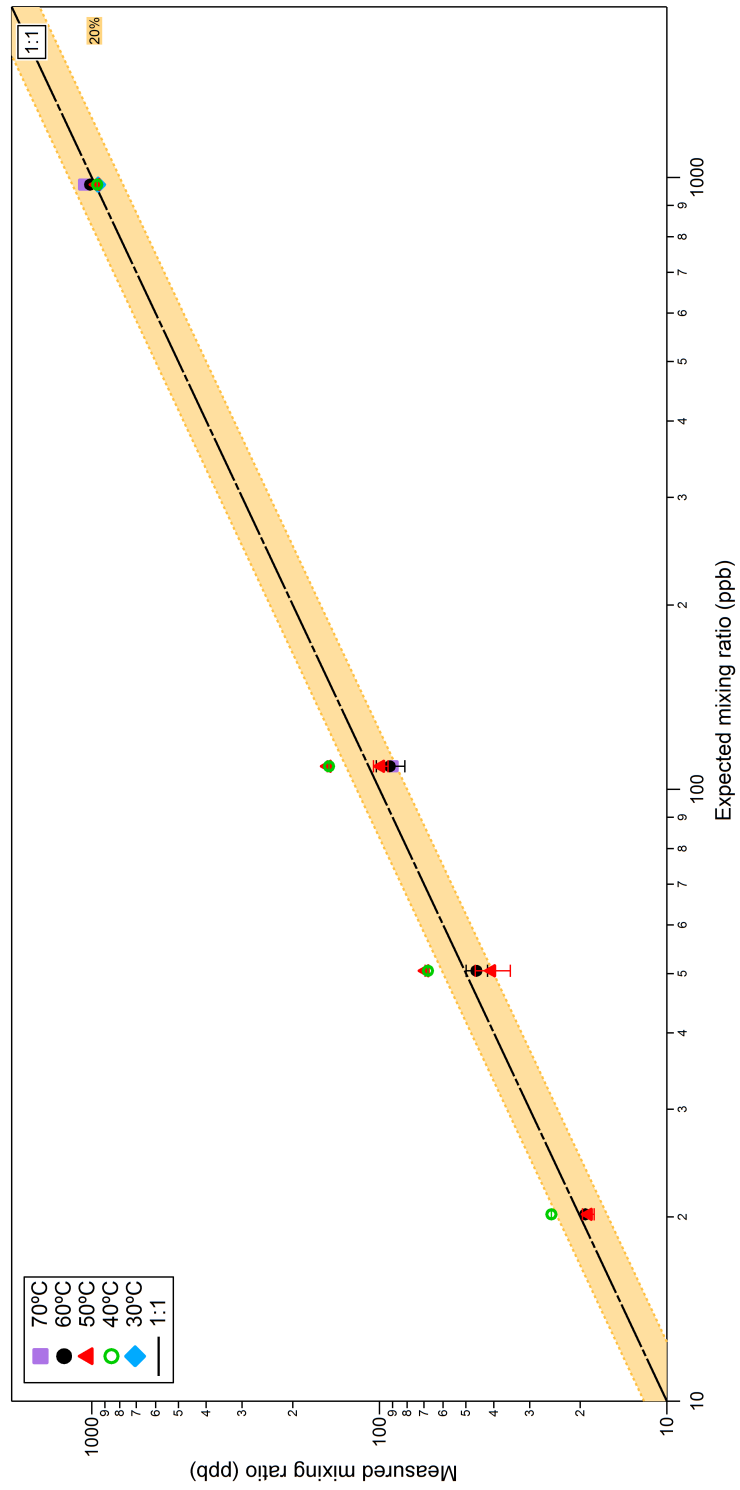


Figure 3.3. P-xylene: measured concentration against expected concentration for a temperature range of $[T=30^{\circ}\text{C} : T=70^{\circ}\text{C}]$

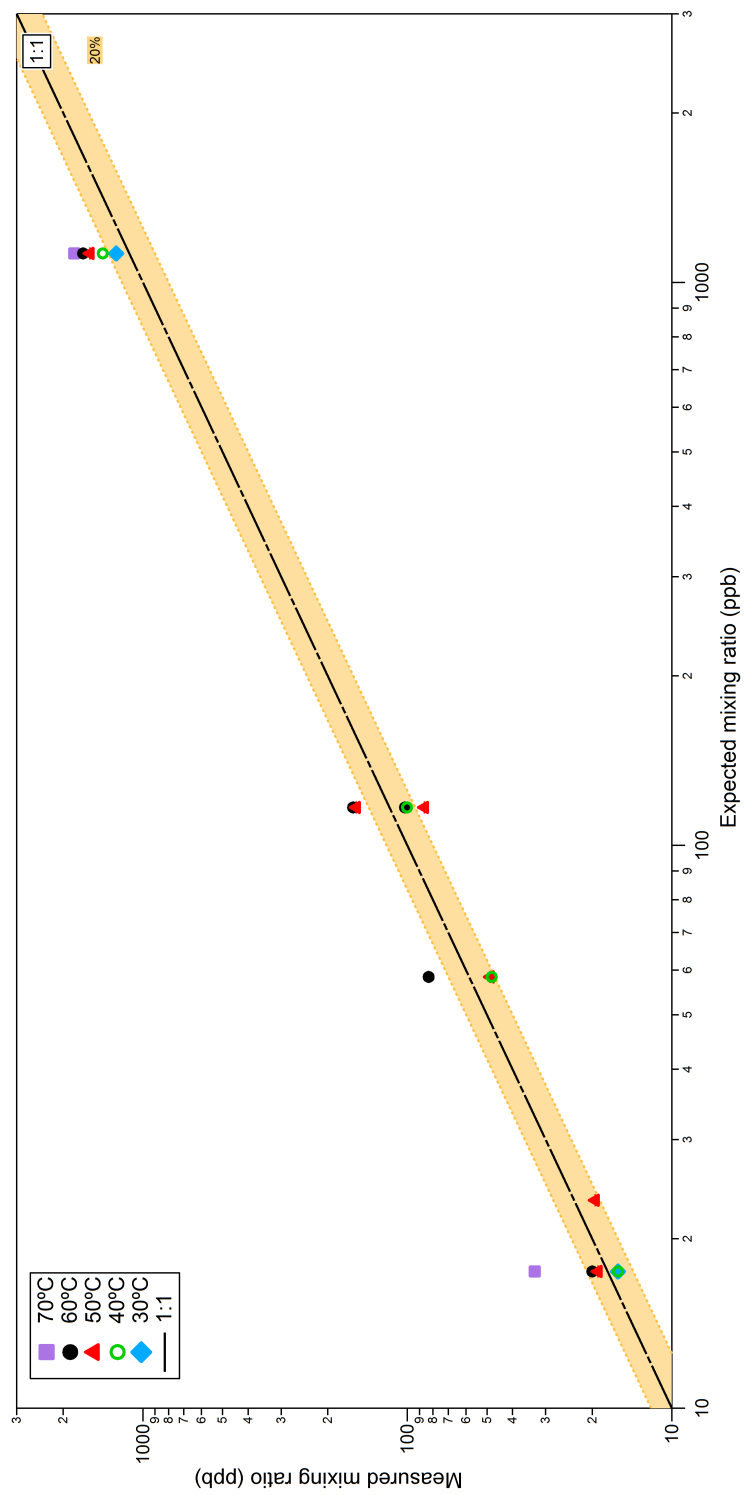


Figure 3.4. Toluene: measured concentration against expected concentration for a temperature range of $[T=30^{\circ}\text{C} : T=70^{\circ}\text{C}]$

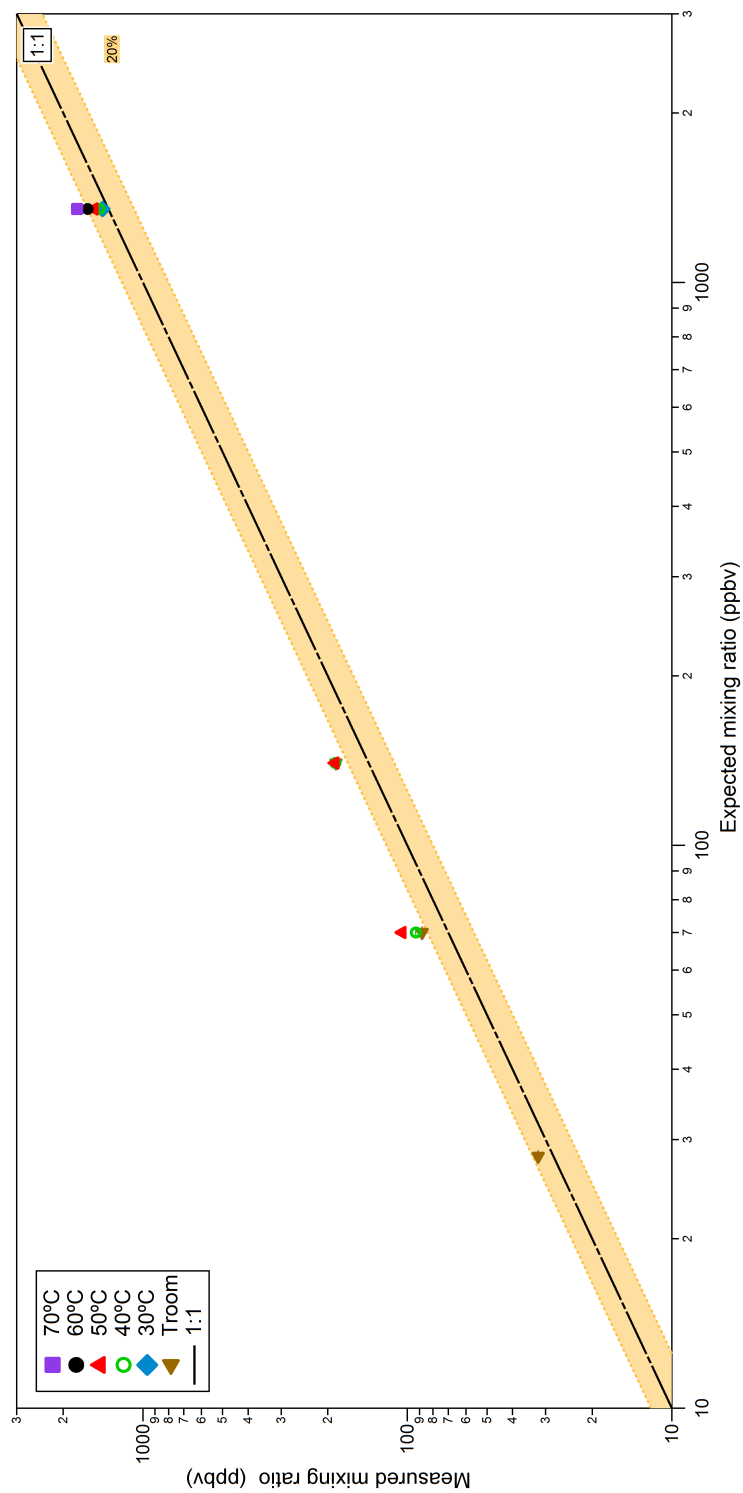


Figure 3.5. Benzene: measured concentration against expected concentration for a temperature range of $[T_{room} : T=70^{\circ}\text{C}]$

do not exist in calibration tanks. The good accuracy of the dynamic dilution system for the lower vapor pressure compounds, p-xylene and trimethylbenzene, permits to assume that for mixtures of PAHs introduced in the system the measured mixing ratio corresponds to the expected mixing ratio providing the required value to calculate their sensitivities.

3.1.4 PAH sensitivities

The sensitivities for acenaphthene, acenaphthylene and biphenyl were tested using the dynamic dilution system heated up to 85°C to avoid wall deposition of those heavy compounds. These compounds are solid at atmospheric conditions so a solution with dichloromethane was made (100 mg into 200 mL). The N₂ dilution flow varied between 1.1 slpm and 5.1 slpm, and the injection rate varied between 20 $\mu\text{l hr}^{-1}$ and 50 $\mu\text{l hr}^{-1}$ to obtain different ranges of concentration. As the accuracy of the dynamic dilution system has been proved, especially for lower vapor pressure compounds, it is assumed that the expected concentration corresponds to the measured concentration. The sensitivities S_i obtained is the fraction of the measured normalized counts NC (in Hz per MHz H₃O⁺) over the expected concentration in ppbv. The resulting average sensitivities are summarized in Table 3.4.

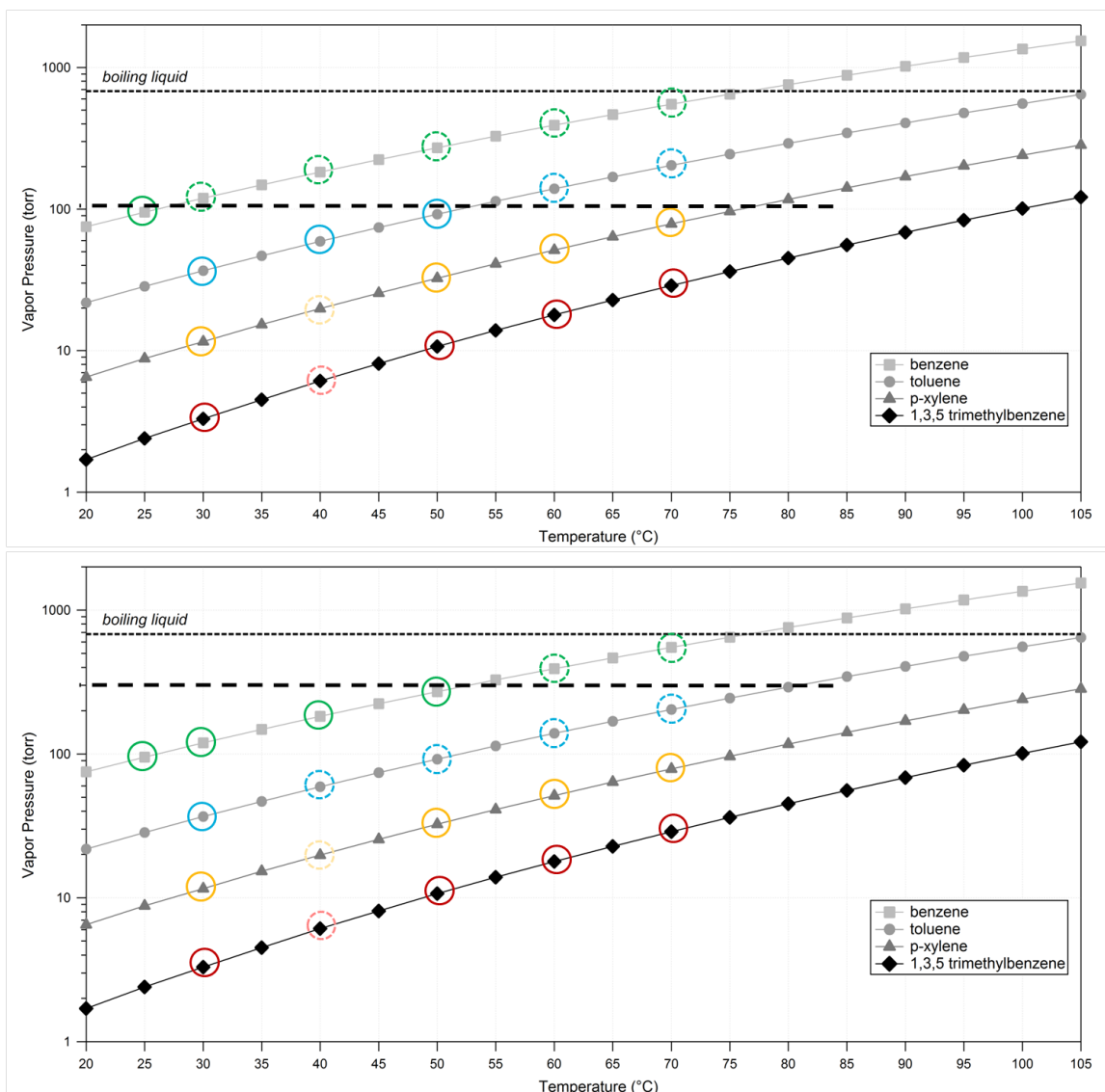


Figure 3.6. Upper limit of vapor pressures for: benzene, toluene, p-xylene and 1,3,5-trimethylbenzene. Top: Infusion rate less than $0.5 \mu\text{l hr}^{-1}$. Bottom: Infusion rate of $5 \mu\text{l hr}^{-1}$.

Table 3.4. PAHs sensitivities at Td80

compounds (MW+1)	sensitivities (NCPS)	stdv
Acenaphthylene (153)	3.1	0.3
Acenaphthene (155)	3.2	0.3
Biphenyl (155)	3.2	0.6

3.2 Fragmentation: dissociative proton transfer reactions

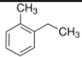
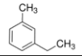
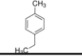
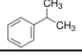
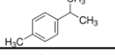
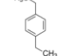
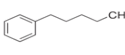
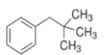
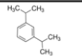
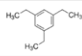
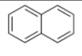
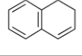
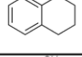
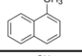
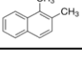
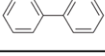
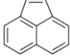
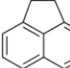
3.2.1 Fragmentation Patterns of Aromatic Compounds

Dissociative proton transfer reactions can occur in the drift tube of the PTR-MS causing the formation of lower mass fragment ions. It is known that the degree of dissociation that occurs is a function of the E/N value; higher Townsend operation implies larger H_3O^+ kinetic energy. The collision energy of the reaction and resulting collisions of the RH^+ product ion with the bath gas can cause dissociation. The geometry and functional groups attached to the compound are important parameters in determining the extent of fragmentation and the likelihood that a compound can be detected at the RH^+ product ion mass. The fragmentation of alcohols, aldehydes, ketones and esters compounds has been well documented in the literature (34). While fragmentation of light aromatic compounds is known, little is known about the fragmentation of larger alkyl substituted aromatic compounds found in diesel engine exhaust. The dissociation products may distort the measurements of a sample composition, overvaluing the concentration of the products resulting from fragmentation and underestimating the concentration of the actual compounds present in the sample. A clear understanding of the dissociation reactions is important for interpreting the accuracy of PTR-MS measurements, especially for complex mixtures found in exhausts and ambient air. For our study, some aromatic compounds that are present in gasoline and diesel engine exhausts, from a molecular weight of 120 g mol^{-1} to 154 g mol^{-1} with different molecular structures, were selected and injected separately in the PTR-MS at Townsend numbers of 80, 100, 120 and 150. The aim of these experiments was to understand which types of species are likely to fragment into which

products, and to quantify their fragmentation patterns. The studied compounds and their molecular structures are listed in Table 3.5 and ordered by molecular weight. The purity of the compounds ranged from 89% to 99.5%. Also, some of the compounds are solids at room temperature conditions of the laboratory so were dissolved in dichloromethane. The composition and the dilution ratio of the compounds studied for fragmentation are summarized in Table 3.5. To organize the results the aromatic compounds have been classified into the four following families: monocyclic aromatic hydrocarbons, PAHs, naphthalene and structurally related compounds, and biphenyl.

The monocyclic aromatic hydrocarbons group corresponds to a single benzene ring (6 carbon atoms) with an alkyl group attached to it. It is known that some of these compounds fragment. For example ethylbenzene, a common constituent in urban air, partially fragments to produce an ion at $m/z=79$ and $m/z=107$ (32). Fragmentation of ethylbenzene causes a positive interference for measuring benzene at $m/z=79$. Our hypothesis is that monocyclic aromatics with ethyl, propyl, or butyl groups attached to the ring may be prone to dissociation. Fragmentation of high molecular weight monocyclic aromatics found in diesel fuel and exhaust may produce interfering fragment ions for both benzene and toluene ($m/z=93$). Also of interest is whether fragmentation of alkyl substituted monocyclic aromatics would produce ions at the series $m/z=43, 57, 71, 85, 99$. These ions could potentially be used to measure the abundance of alkanes (35) and thus would produce a positive interference. In contrast to the monocyclic aromatics, the poly aromatic compounds are not thought to fragment though this has not been reported in the PTR-MS relevant literature. Using electron impact ionization fragmentation patterns as a guide, these compounds typically show a strong molecular ion and do not extensively fragment. The biphenyl

Table 3.5. List of compounds tested for fragmentation.

Compound Name	Molecular structure	MW (g/mol)	Chemical purity (%)
Aromatics			
2-ethyltoluene		120	99
3-ethyltoluene		120	99
4-ethyltoluene		120	90
cumene		120	98
p-cymene		134	99
1,4-diethylbenzene		134	96
pentylbenzene		148	99
2,2-dimethyl-1-propylbenzene		148	> 97
1,3-di-isopropylbenzene		162	> 98
1,3,5-Triethylbenzene		162	> 97
Naphthalenes			
Naphthalene		128	> 98
1,2-dihydronaphthalene		130	98
Tetrahydronaphthalene		132	> 98
1-methylnaphthalene		142	> 98
1,2-dimethylnaphthalene		156	95
Biphenyls			
Biphenyl		154	> 98
PAHs			
Acenaphthylene		152	89,8 (Acenaphthene 9.8%)
Acenaphthene		154	99,5

group structures are based on two benzene rings connected by a carbon-carbon single bond. Alkyl groups may be attached to the benzene rings forming a range of structurally similar compounds. The hypothesis is that fragmentation will occur at this common carbon bond. The naphthalene group consists of organic compounds that are composed of two fused benzene rings with alkyl groups attached to the 2 rings. For the naphthalene and structurally related compounds, the hypothesis is that no fragmentation occurs, similar to what is observed with electron impact ionization. To simplify the reporting of the general fragmentation patterns, only the masses that were more than 10% of the total ion signal in the raw data were considered as significant fragmentation products for further analysis. For the data presented the measured ion count rates are reported. Since the solid compounds were dissolved in dichloromethane (CH_2Cl_2), a high concentration dichloromethane test mixture was prepared with the dynamic dilution system to obtain a background fragmentation pattern. As shown in Figure 3.7, the dichloromethane mass spectrum shows ions at $m/z=31$, $m/z=49$, $m/z=51$. The $m/z=31$ does not correspond to any known C_xH_y compounds but could correspond to the CH_3O^+ compound from some reactions occurring in the ion source (36). A possible mass assignment for $m/z=49$ and $m/z=51$ is CH_2Cl^+ which implies ionization of the CH_2Cl_2 solvent and loss of a Cl-atom. The $m/z=49$ ion corresponds to the ^{35}Cl isotope and while the $m/z=51$ ion contains the ^{37}Cl isotope. The signal of $m/z=49$ is 3 or 4 times higher than the $m/z=51$ signal, which corresponds to the isotopic abundance of ^{35}Cl and ^{37}Cl . CH_2Cl_2 does not react with H_3O^+ so its ionization and fragmentation is likely occurring in the ion source rather than in the drift tube. Given the low pressure difference between the ion source and the drift tube, it is known that air sample can diffuse into the ion source

creating unwanted secondary ions such as O_2^+ and NO^+ . The ions $m/z=31, 49, 51$ were not included in the fragmentation study of dissolved compounds. The CH_2Cl_2 mass spectrum had other ions at a lower abundance ($m/z=29, 47, 67, 69$), and while it is not clear how these arise, these were also considered to be solvent background ions and not included in the fragmentation study. The percentages presented below are calculated by ignoring the ^{13}C isotopes masses measured in the samples. The percentages are summarized into Table 3.6, and are illustrated for both Td80 and Td150 in Figure 3.13 and Figure 3.14.

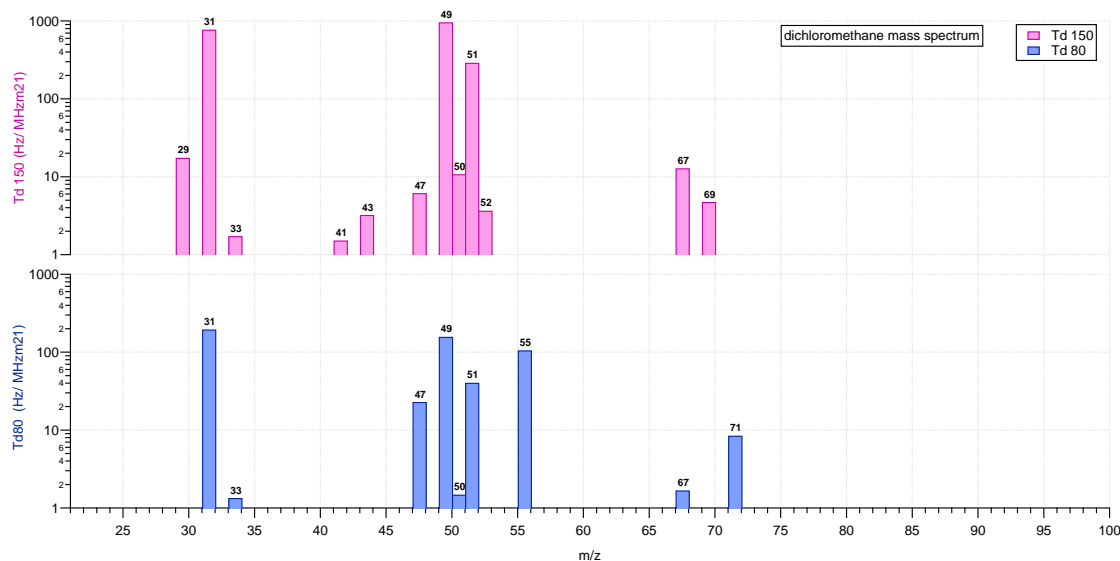


Figure 3.7. Mass spectra of the dichloromethane at Td80 and Td150

3.2.1.1 Monocyclic aromatic hydrocarbons

The compounds 2-ethyltoluene, 3-ethyltoluene and 4-ethyltoluene have a molecular weight of 120 g mol^{-1} , so produce a RH^+ ion at $m/z=121$. They are all composed of a benzene ring with a methyl group and an ethyl group attached to it. They differ

by the position of the ethyl group attached to the benzene ring. The results for these three compounds were similar and the fragmentation occurred the same way. For Td80 and Td100 there was no dissociation, at Td120 the compounds fragmented producing an ion at $m/z=93$ (protonated toluene) with a 4% yield. At Td150 the compounds fall apart resulting in $62\pm3\%$ of the ion signal at $m/z=93$ and only $38\pm3\%$ at $m/z=121$. Thus, fragmentation of these compounds at higher Td values would produce positive interferences for the measurement of toluene. The fragmentation pattern implies that the ethyl group attached to the benzene group falls off, but not the methyl group. The significant fragmentation for those compounds reduces the measured signal of $m/z=121$ and increases the $m/z=93$ ion signal at higher Td values.

The compound 1,4-diethylbenzene has a MW of 134 g mol^{-1} , so produces an RH^+ ion at $m/z=135$. It is composed of two ethyl groups attached to a benzene ring. At Td80 and Td100 no dissociation was observed. At Td120 fragment ions at $m/z=79$ and $m/z=107$ appeared, accounting for 7% and 3% of the total ion signal respectively. At Td150 the 1,4-diethylbenzene significantly dissociates, only $41\pm3\%$ of the signal corresponds to $m/z=135$, whereas the $m/z=79$ and $m/z=107$ account for $52\pm3\%$ and 8% of the total ion signal respectively. This means that either both of the ethyl groups or one of them fall off the benzene ring, reducing the measured counts of $m/z=135$ and increasing the $m/z=79$ and $m/z=107$ counts.

Cumene is a compound found in refined fuel and crude oil (37). It has a MW of 120 g mol^{-1} , so it is measured at $m/z=121$. The compound structure is an isopropyl group attached to a benzene ring and is also known as isopropyl benzene. At Td100, the cumene compound fragments significantly to $m/z=79$; the percent of the signal at $m/z=121$ and $m/z=79$ was respectively 36% and 60%. About 4% of the signal

occurred at $m/z=41$. At Td120, the fragmentation is larger so that the percent for $m/z=121$ drops to 9% of the total ion signal, whereas the percent of $m/z=79$ and $m/z=41$ increases to 67% and 24%. At Td150 $m/z=79$ and $m/z=41$ are the major ions accounting for 49% and 26% of the ion signal respectively, with $m/z=121$ accounting for 3%. The ion at $m/z=41$ is likely to be $C_3H_6^+$, the product ion from the isopropyl (C_3H_7) fragmentation. The test shows that the isopropyl group is likely to fragment from the ring even at a low Townsend number (Td100) producing a positive interference for the measurement of benzene at $m/z=79$.

The compound p-cymene has a MW of 134 g mol^{-1} , so produces a RH^+ ion measured at $m/z=135$. It is a benzene ring with a methyl group and an isopropyl group attached to it and thus structurally similar to cumene. At Td80 there is already a significant dissociation into $m/z=93$ that occurs; the signal at $m/z=135$ and $m/z=93$ are respectively $90\pm1\%$ and $10\pm1\%$. At Td100, the fragmentation increases, so that the percent of $m/z=135$ drops to 55% of the signal and the $m/z=93$ ion represents 45% of the signal. At Td120 the $m/z=135$ ion is only $10\pm1\%$ of the total ion signal and $m/z=93$ accounts for $90\pm1\%$. At Td150, $m/z=135$ is just $2\pm1\%$ of the signal, $m/z=91$ represents 6%, $m/z=41$ represents 4%, and $m/z=93$ is the main ion representing $84\pm2\%$ of the signal. The data suggests the isopropyl group attached to the benzene ring is likely to fall off even at Td80 and for higher Townsend numbers the $m/z=135$ may be barely present in the signal. The methyl group does not seem to break off because no benzene ion ($m/z=79$) was measured. Fragmentation of this compound thus produces interference for measuring toluene. Its fragmentation pattern was very similar to cumene. Results from measuring p-cymene and cumene suggest the isopropyl group is susceptible to loss from the benzene ring.

The compound 1,3,5-triethylbenzene has a MW of 162 g mol⁻¹, so is measured at m/z=163. It is composed of 3 ethyl groups attached to a benzene ring. At Td80, Td100 and Td120 1,3,5-triethylbenzene does not fragment significantly and the m/z=163 ion represents 100%, 100% and 94% of the signal respectively. At Td150 dissociation is observed, so that m/z=163 ion comprises 80±3% of the total ion signal. The fragment ions were m/z=79 and m/z=135 that represent respectively 5±2% and 4±1% of the signal and related geometric isomers are unlikely to produce interferences for the measurement of lighter aromatics. It shows that either the three ethyl groups fragment off the compound leaving behind a protonated benzene ring, or only one ethyl group leaves so that a protonated diethylbenzene compound is measured. The noticeable increase in m/z=55 is representative of the formation of water clusters.

The compound 1,4-di-isopropylbenzene with a RH⁺ ion of m/z=163 is composed of a benzene ring with two isopropyl groups attached, structurally similar to cumene and p-cymene. At Td80, m/z=163 is the dominant ion accounting for 93±12% of the total ion signal. Some m/z=39 is also already present by 12% of the signal in one of the sample. At Td100, m/z=163 is still dominant at 78±4%; m/z=43 appears in a significant amount at 11±1% of the signal. Ions at m/z=79 as m/z=39 are also present at 7% and 8% respectively of the signal. At Td120 dissociation is observed, so that m/z=43, m/z=79 and m/z=41 represent respectively 35±3%, 32% and 11±1% of the total ion signal and m/z=163 represents only 19% of the signal. At Td150, m/z=79 is the main ion representing 38±3% of the signal and m/z=163 is only 2% of the signal. Other major ions are m/z=41, m/z=39 and m/z=43 accounting for 24%, 23%, and 12% respectively. For this compound, we can say that the isopropyl

branches fragment off and only the benzene ring is measured for Townsend number higher than 100. The increase in smaller masses $m/z=39$, $m/z=41$ and $m/z=43$ become significant as the Townsend number increases. The ion at $m/z=41$ is likely to be the product ion from the isopropyl fragment. The dissociation into $m/z=43$, $C_3H_7^+$, is important to notice because it is an ion used to measure the abundance of alkanes. The $m/z=39$ corresponds to the water cluster formation, it is the mass for the $H^+(H_2O)_2$ ion, as formed in equation 2.3. Formation of water clusters would be expected at lower Townsend values through reaction 2.2 and 2.3 In these experiments the m/z 39 ion increased with higher Td numbers suggesting it is not a water cluster ion but an organic ion. This ion mass is observed in electron impact ionization of aromatic compounds (38) and so it is suspected that this is an organic ion resulting from decomposition of the aromatic ring.

Both pentylbenzene and 2,2-dimethyl-1-propylbenzene have a MW of 148 g mol^{-1} , and would be measured at $m/z=149$. The two compounds present similar results so are discussed together. Both are composed of a straight chain alkyl group attached to a benzene ring. This alkyl group is respectively a 5 carbon alkyl chain (pentyl group) and a 3 carbon alkyl chain (propyl group). At Td80, $m/z=149$ represents 100% of the signal for both species. At Td100, the pentylbenzene is still largely represented by $m/z=149$ at 89% of the signal, and $m/z=43$ and $m/z=39$ are also measured representing respectively 8% and 3% of the signal. For the 2,2-dimethyl-1-propylbenzene, $m/z=149$ is representative of only $36\pm1\%$ of the signal whereas $m/z=43$ counts increase so that it represents $62\pm2\%$ of the signal, and $m/z=39$ is 4% of the signal. At Td120 the percent of $m/z=149$ in the signal goes down for both species (to $11\pm5\%$ and 2%) so that $m/z=43$ and $m/z=41$ become the main masses measured representing

respectively 67% and $19\pm5\%$ of the signal for pentylbenzene and $78\pm1\%$ and $21\pm1\%$ of the signal for 2,2-dimethyl-1-propylbenzene. At Td150 the signal is not represented by $m/z=149$ anymore, but by the group of $m/z=39$, $m/z=41$, and $m/z=43$. For pentylbenzene $m/z=39$, $m/z=41$, and $m/z=43$ represent respectively $35\pm10\%$, $32\pm2\%$ and $16\pm2\%$ of the signal, and for 2,2-dimethyl-1-propylbenzene $m/z=41$ and $m/z=43$ are respectively $53\pm19\%$ and $27\pm10\%$. We can notice the interesting break down of those two compounds as the Townsend number increases. There is a little fragmentation into benzene but it is not significant compared to the detected amount of $m/z=39$, $m/z=41$ and $m/z=43$. The $m/z=39$ ion is likely an organic ion from the decomposition of the aromatic ring and not a water cluster, and $m/z=41$ is likely to come from the fragment of the alkyl chain. These compounds are likely to have a positive interference with the measurements for alkanes due to the dissociation into $m/z=43$.

3.2.1.2 *Naphthalenes*

Naphthalene is a solid at ambient temperature, so it was dissolved into dichloromethane at a concentration of 200 mg into 100 mL of solvent. This compound is composed of two benzene ring stuck together with a MW of 128 g mol^{-1} so it is measured at $m/z=129$. For this compound the signal of $m/z=129$ is detected, but it is low compared to $m/z=49$ and $m/z=31$ as shown on the barscan in Figure 3.8. We can see a small decrease in the signal from Td80 to Td120 that can be due to the sensitivity of the PTR-MS at Td120.

The compound 1,2-dihydronaphthalene has a MW of 130 g mol^{-1} , so is measured at $m/z=131$. This compound is a naphthalene compound that has one of its benzene

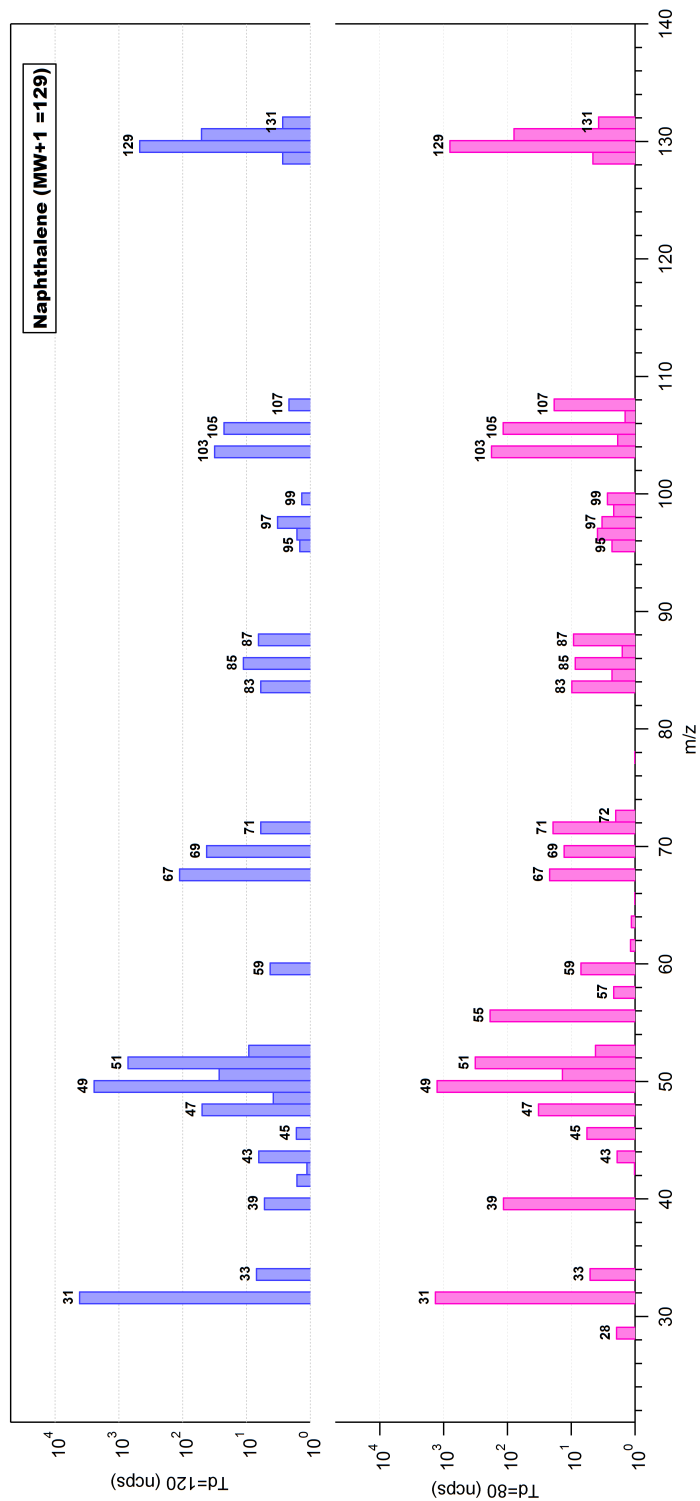


Figure 3.8. Fragmentation of naphthalene: barscan

ring partially saturated so two additional hydrogen atoms are attached. This compound does not present any fragmentation phenomenon for any Townsend number from 80 to 150. As we can see on the 1,2-dihydronaphthalene barscan in Figure 3.9, there is a little increase in the ion signal at $m/z=91$, but this is not significant enough to count as a fragment.

The compound tetrahydronaphthalene has a MW of 132 g mol^{-1} , so is measured at $m/z=133$. It is a naphthalene compound that has one of its benzene ring saturated so four additional hydrogen atoms are attached. At Td80 and Td100, $m/z=133$ represents 100% of the signal. At Td120 $m/z=133$ is 93% of the total signal with $m/z=91$ accounting for 7%. The $m/z=91$ ion is a common fragment ion of aromatic compounds observed in electron impact ionization and corresponds to the very stable benzyl ion C_7H_7^+ or tropylium ion (36,38). At Td150 $m/z=91$ and $m/z=133$ represent, respectively, 76% and 24% of the signal. We conclude that at higher Td this compound will fragment to produce $m/z=91$ ion.

The compound 1-methylnaphthalene has a MW of 142 g/mol and is measured at $m/z=143$. This compound is naphthalene with a methyl group attached to the ring. For all Townsend numbers from 80 to 150 no fragmentation occurs, and the ion at $m/z=143$ represents 100% of the signal.

The 1,4-dimethylnaphthalene is a naphthalene with two methyl group attached to one of the benzene ring. It has a MW of 156 g mol^{-1} , so it is measured at $m/z=157$. The results show that this compounds does not fragment.

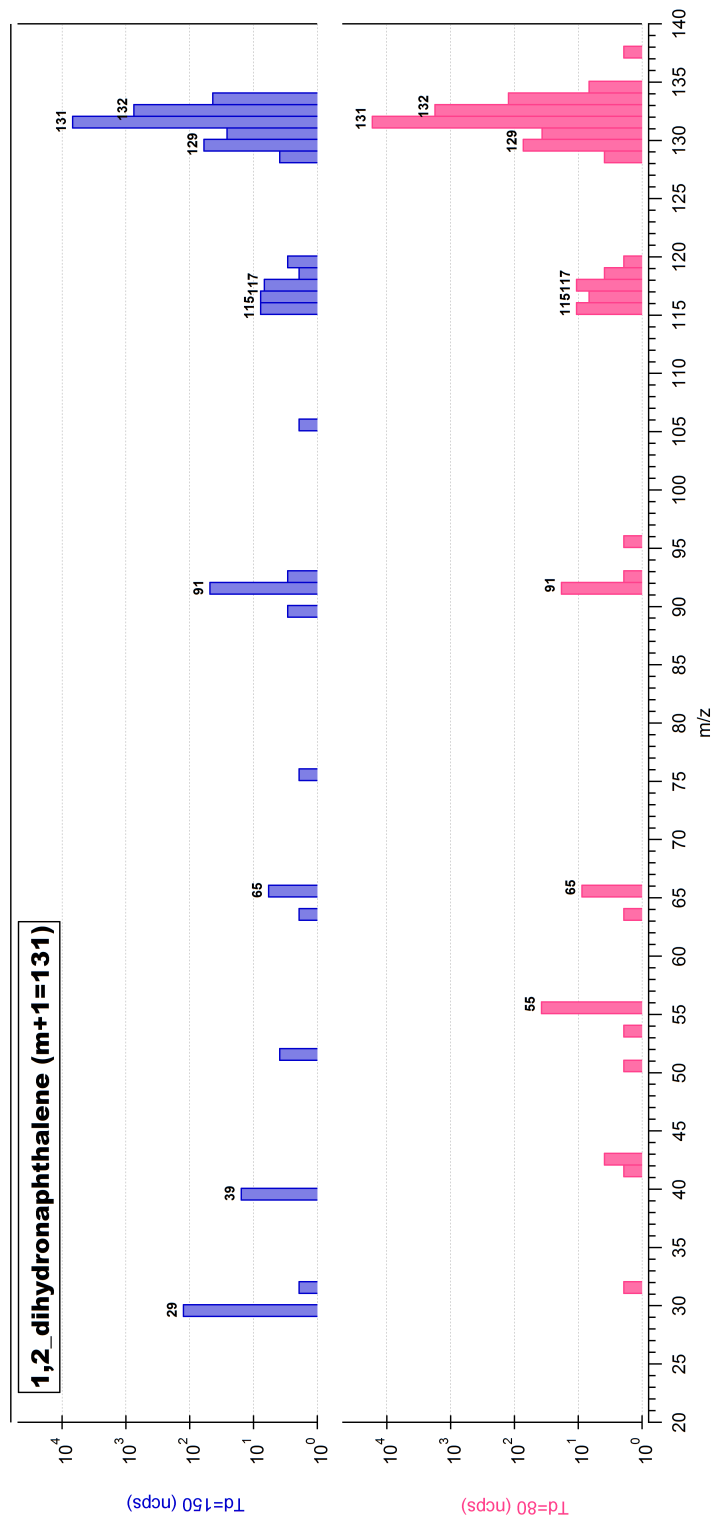


Figure 3.9. Fragmentation 1,2-dihydronaphthalene: barscan

3.2.1.3 PAHs

The PAHs tested were solids at ambient temperature, so were dissolved into dichloromethane. Acenaphthylene ($C_{12}H_8$) is a common compound of coal tar composed of naphthalene with an ethylene bridge linking the two rings. It has a MW of 152 g mol^{-1} so is measured at $m/z=153$. For this compound the signal of $m/z=153$ is detected, but it is low compared to $m/z=49$ and $m/z=31$ as shown on the barscan in Figure 3.10. Those are assumed to come from the solvent, so that no fragmentation pattern is observed for the acenaphthylene.

Acenanphthene ($C_{12}H_{10}$) is a hydrogenated form of the acenaphthylene. It has a MW of 154 g mol^{-1} so is measured at $m/z=155$. Similar to the acenaphthylene compound, the $m/z=155$ ion represents a small percent of the signal compared to $m/z=49$ and $m/z=51$ that come from the solvent solution as shown on the barscan in Figure 3.11. There is also an increase in $m/z=29$ that will be considered to come from the solvent solution. But the $C_2H_5^+$ ions might also form by fragmentation (36).

3.2.1.4 Biphenyl

Biphenyl is a compound with a MW of 154 g mol^{-1} so measured at $m/z=155$. This compound is also solid at ambient temperature so it was dissolved into dichloromethane. The $m/z=155$ represents a small percent of the signal compared to the $m/z=31$ and $m/z=49$ that comes from the solvent composition as shown on the barscan in 3.12. The biphenyl does not show significant fragmentation as expected.

3.2.2 Fragmentation Pattern Summary

The percent abundance of the compounds fragmenting are given in Figure 3.13, Figure 3.14 and Figure 3.15. The main conclusions from the fragmentation tests are the following:

1. The ethyl groups attached to a benzene ring are likely to fall off at Td150.
2. The isopropyl groups attached to a benzene ring are likely to fall off easily, from Td80 and even more at higher Townsend numbers (Td120 and Td 150).
3. The methyl groups attached to a benzene ring do not seem to fall off.
4. The dissociation of the compounds with longer groups attached to the benzene ring such as pentylbenzene, 2,2-dimethyl-1-propylbenzene and 1,3-di-isopropylbenzene are likely to produce a positive interference in the measurement of alkanes.
5. For the two PAHs, the naphthalenes (except the tetrahydronaphthalene), and biphenyl no significant fragmentation occurs.

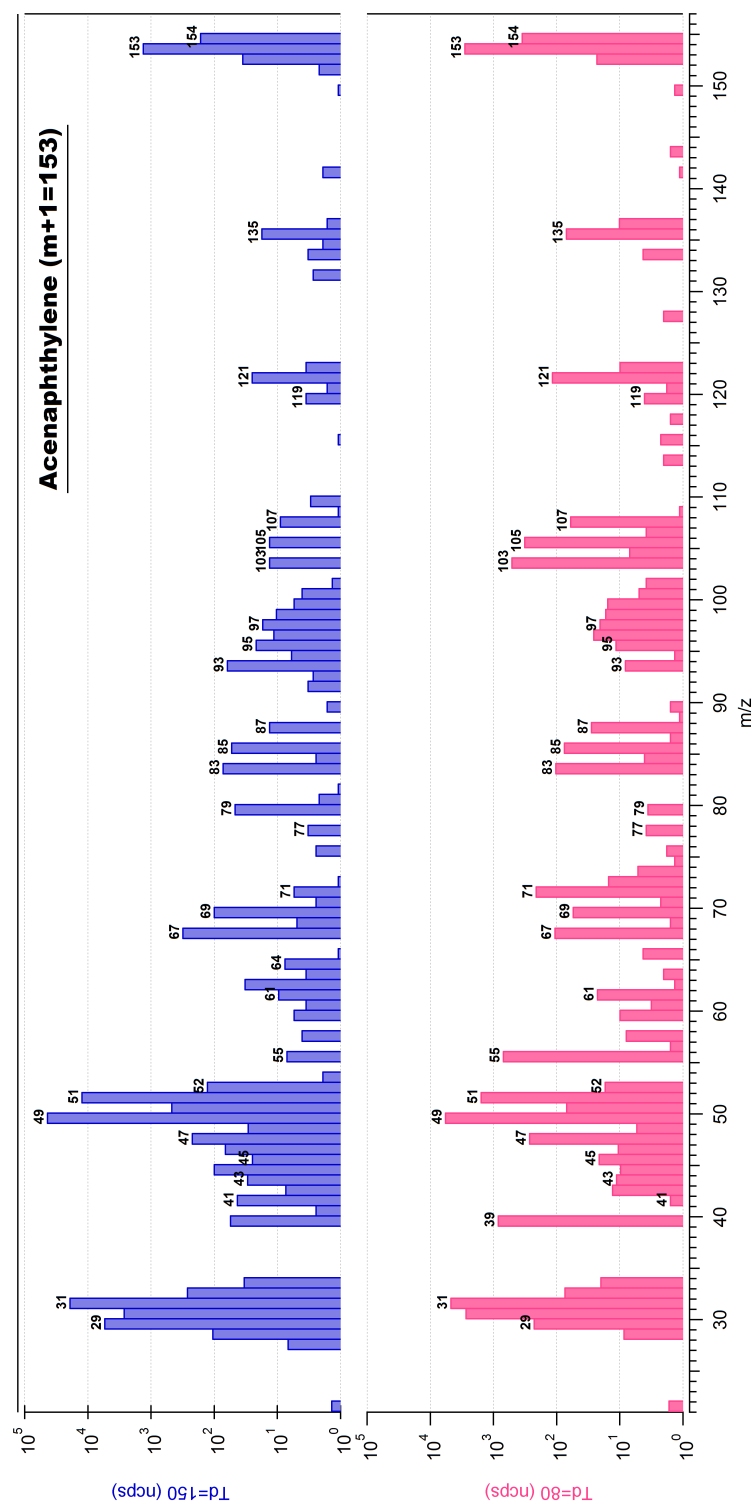


Figure 3.10. Fragmentation acenaphthylene: barscan

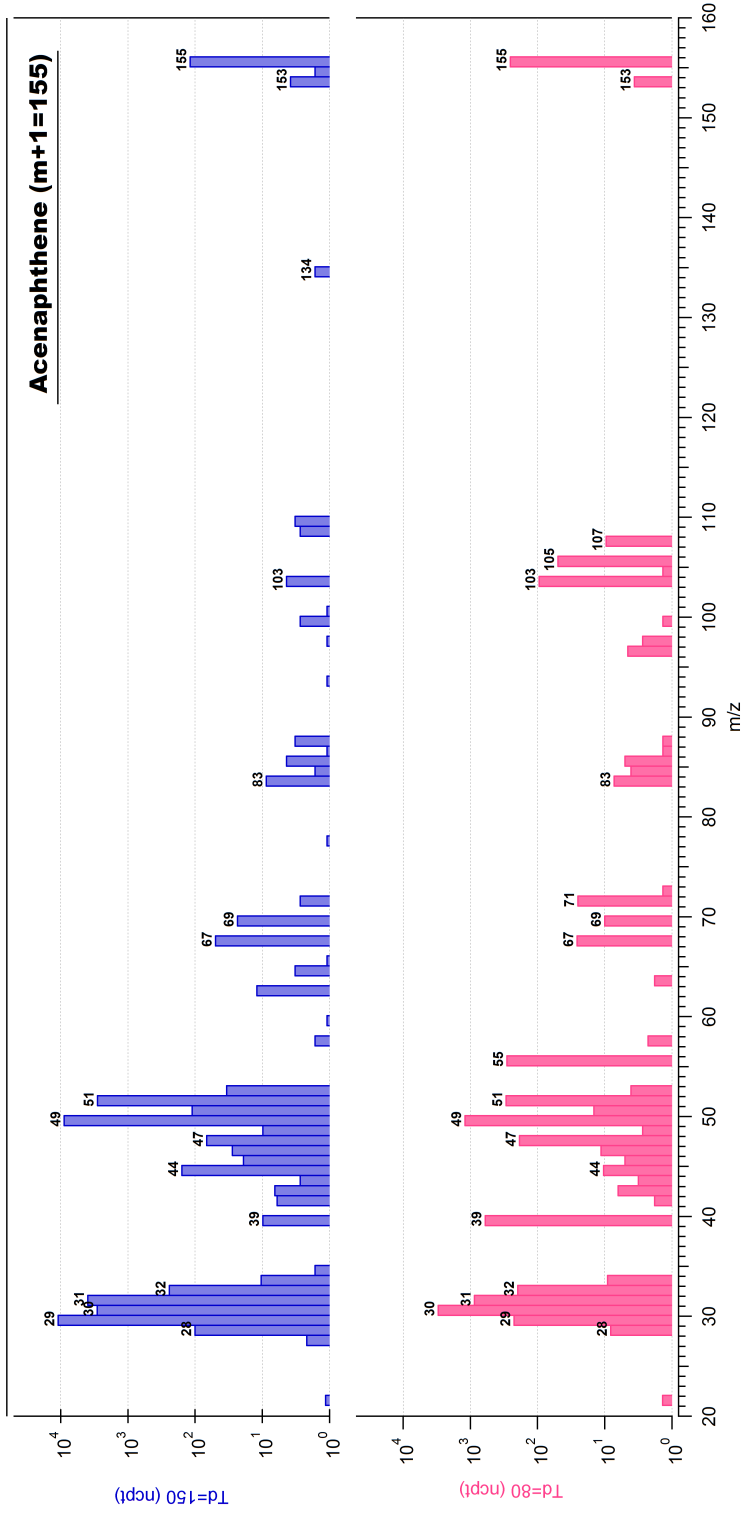


Figure 3.11. Fragmentation acenaphthene: barscan

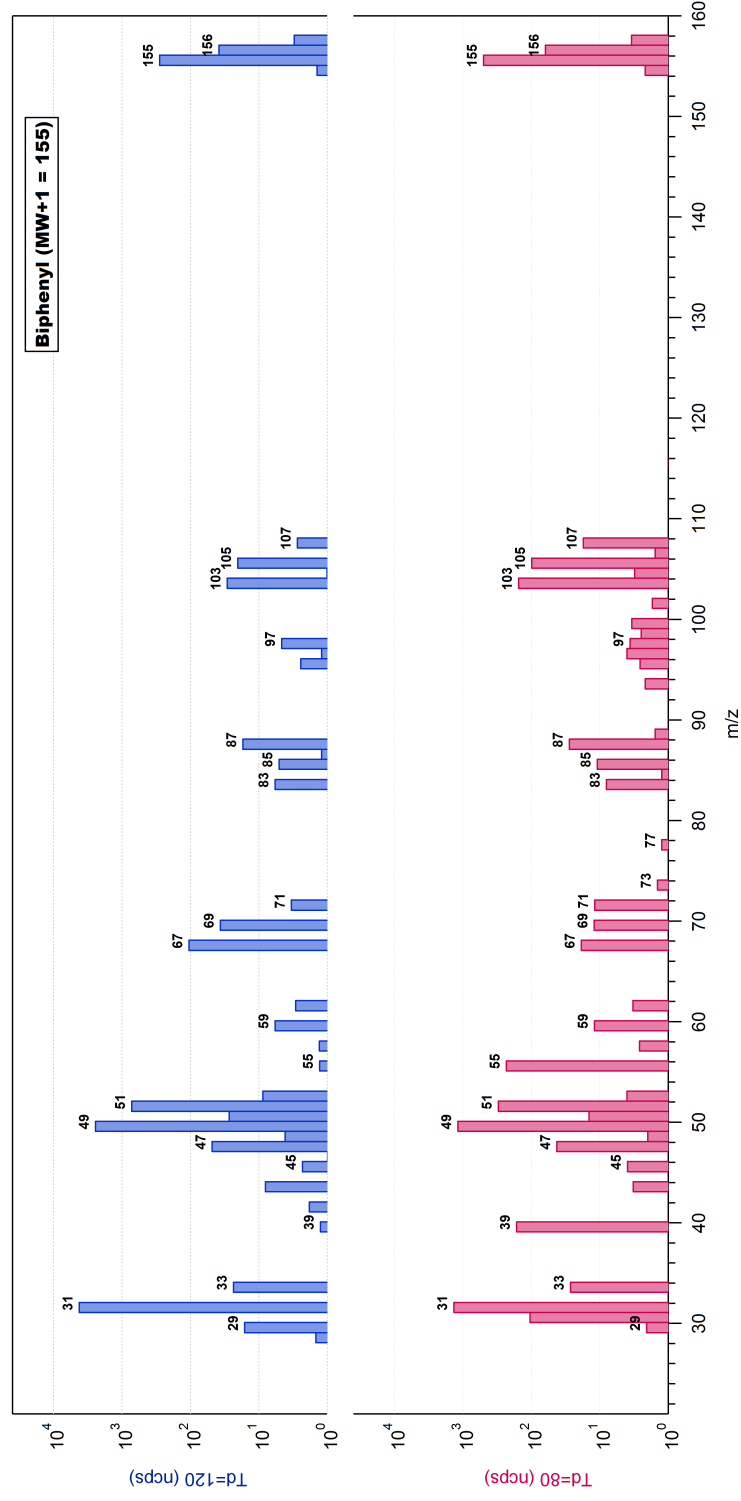


Figure 3.12. Fragmentation biphenyl: barscan

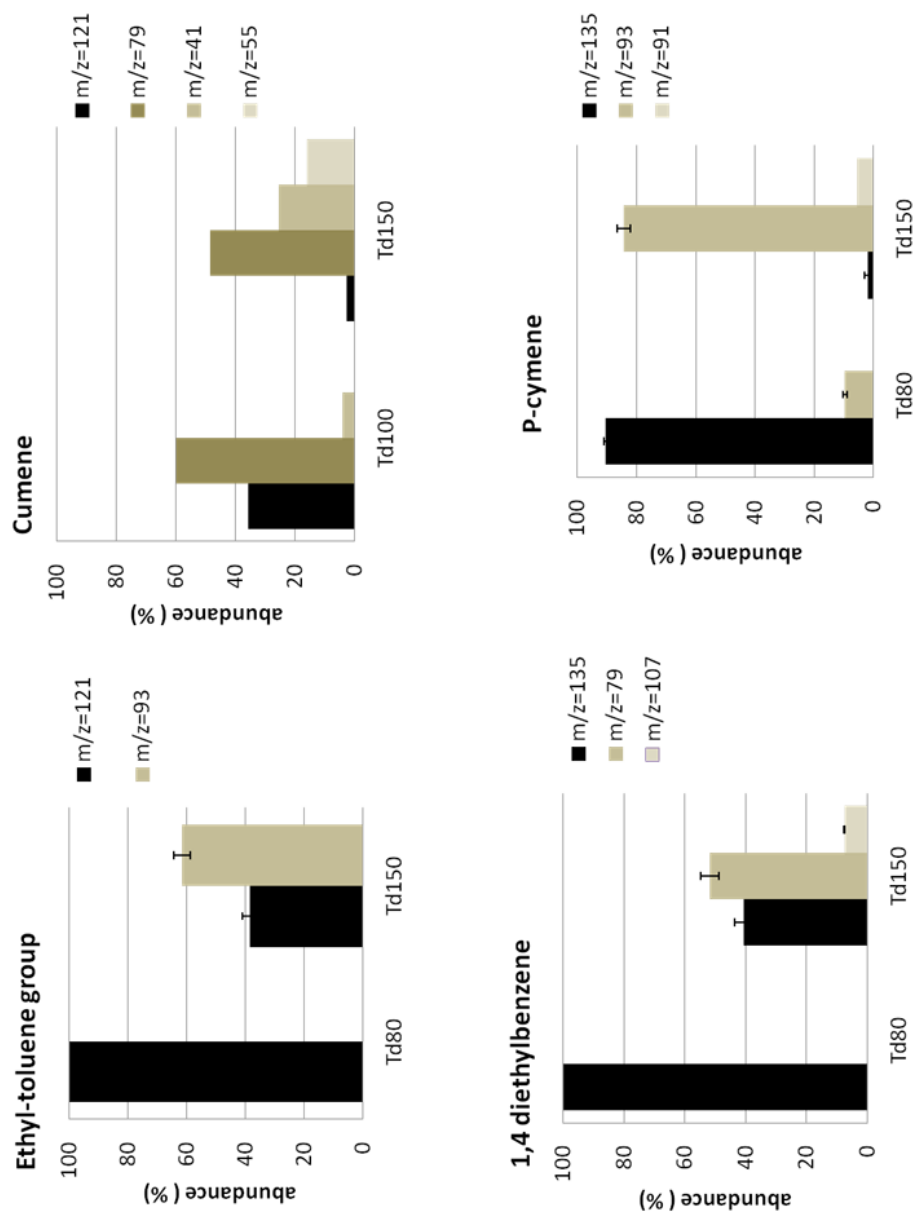


Figure 3.13. Fragmentation abundance (%)

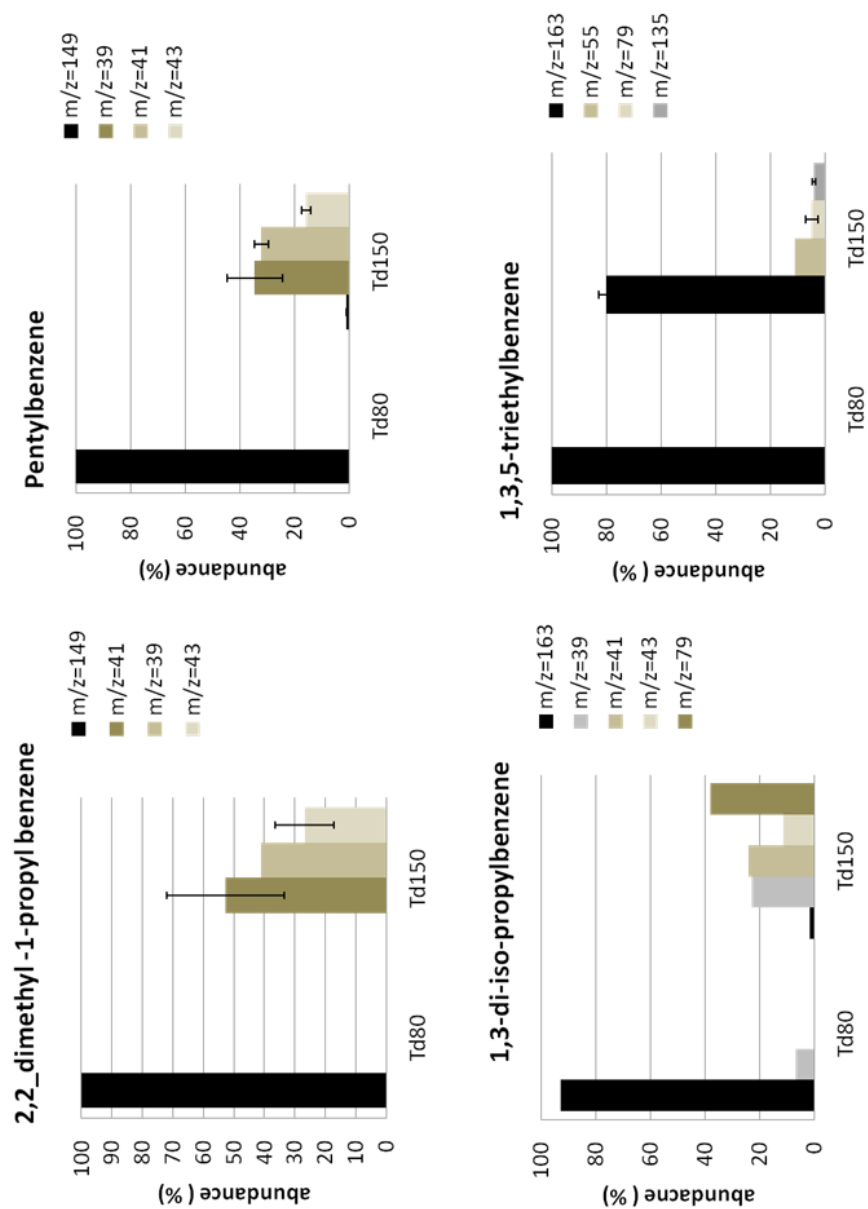


Figure 3.14. Fragmentation abundance (%) (continued)

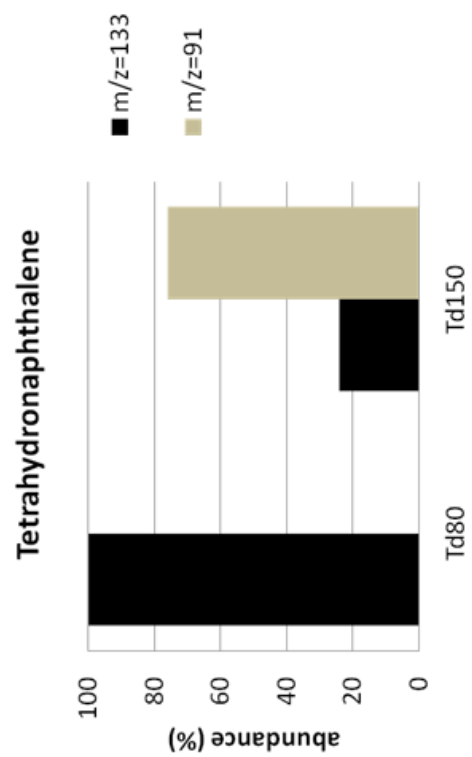


Figure 3.15. Fragmentation abundance (%) (continued)

Table 3.6. Fragmentation

Compound Names (MW+1)	Composition								
	Td=80			Td=100			Td=150		
	m/z	Td80	% STDV	m/z	Td100	% STDV	m/z	Td150	% STDV
AROMATICS									
2-ethyltoluene (121)	121	100	0	121	100	0	93 121	62 38	3 3
3-ethyltoluene (121)	121	100	0	121	100	0	93 121	62 38	3 3
4-ethyltoluene (121)	121	100	0	121	100	0	93 121	62 38	3 3
cumene (121)				79 121 41	60 36 4		79 41 55 59 80 121	49 26 16 4 3 3	
p-cymene (135)	135 93	90 10	1 1	135 93	55 45		93 91 41 135	84 6 4 2	2 0 0 1
1,4-diethylbenzene (135)	135	100	0	135	100	0	79 135 107	52 41 8	3 3 0
pentylbenzene (149)	149	100	0	149 43 39	89 8 3		39 41 43 27 149	35 32 16 5 1	10 2 2 3 0
2,2-dimethyl-1-propylbenzene (149)	149	100	0	43 149 39	62 36 4	2 1	41 43 39	53 27 41	19 10
1,3-diisopropylbenzene (163)	163 39	93 7	12 12	163 43 79 39	78 11 7 8	4 1 0	79 41 39 43 163 27	38 24 23 12 2 4	3 0 1 0 0
1,3,5-triethylbenzene (163)	163	100	0	163	100		163 55 79 135	80 11 5 4	3 0 2 1
NAPHTALENES									
naphthalene ¹ (129)	129	100					129	100	
1,2-dihydronaphthalene (131)	131	100		131	100		131	100	
tetrahydronaphthalene (133)	133	100		133	100		91 133	76 24	
1-methylnaphthalene (143)	143	100		143	100		143	100	
1,4-dimethylnaphthalene (157)	157	100					157	100	
BIPHENYLS									
biphenyl (155) ¹	155	100					155	100	
PAHs									
acenaphthylene (153)	153	100					153	100	
acenaphthene (155)	155	100					155	100	

¹ Run at Td80 and Td120. The results in the column Td150 corresponds to the results for Td120.

CHAPTER 4. LRRI

4.1 Purpose of the study

The University of Washington School of Public Health was awarded an Environmental Protection Agency grant to establish a Clean Air Research Center to study the impact of roadway emissions on cardiovascular health. The center involves 3 institutions: UW School of Public Health, the Lovelace Respiratory Research Institute (LRRI) in Albuquerque New Mexico, and the Laboratory for Atmospheric Research (LAR) at WSU. The role of LAR was to characterize the composition of engine emissions in animal and human exposure chambers at LRRI and UW. The exposure chambers were characterized using PTR-MS to measure organic gases and an aerosol mass spectrometer (Aerodyne Inc) to measure particle composition. One of the main goals of this project is to simulate the roadway emissions by blending gasoline and diesel engine exhaust and exposing mice and humans to those polluted atmospheres to determine the effect on cardio-vascular health. The first exposure chamber characterization study was performed at LRRI from April 21st to May 13th 2012. There were two parts to the study. The first part focused on the mixing of diesel and gasoline exhaust at different particle concentrations and engine loadings in 1.5 m³ exposure chambers. The second part focused on measurements in a 11.5 m³

Teflon chamber to simulate atmospheric chemical processing of exhaust and creation of secondary organic aerosol. Only the first part of the study is presented in this thesis. The data from the VOC inlet are used for the analysis.

4.2 Exposure chamber experimental set up

The engines and the exposure chambers were located in two different rooms on opposite sides of a hallway. The diesel engine was a 5.5 kW Yanmar diesel electric generator (39) and the gasoline engines were 1996 model 4.3L General Motors V-6 engines (8). The exhaust was brought to the exposure chamber room through steel pipes hanging from the ceiling. Three 1.5 m³ exposure chambers (#4, #5, #6) were used for the experiments. While a test was performed with one of the chambers, the other two ones could be conditioned for the next tests. The experiments have been divided into 3 types according to the exhaust composition: diesel exhaust only, gasoline exhaust only, and mixtures of diesel and gasoline exhaust. In order to avoid cross contamination, chamber 4 was used for the gasoline only tests, chamber 5 and 6 were used for diesel only and mixtures tests. The exhaust flows could be diluted with clean house air before flowing into the respective chambers. Teflon filters were used to collect particles and the filters weighed to determine the extent of exhaust dilution based upon PM mass loading for the pure exhaust flow. The set up of the experiment is illustrated in Figure 4.1.

The particulate matter loading in diesel engine exhaust was much larger than in gasoline engine exhaust. Particle mass concentration in the undiluted diesel exhaust stream was about 400 $\mu\text{g m}^{-3}$ compared to 50 $\mu\text{g m}^{-3}$ for the gasoline engine exhaust.

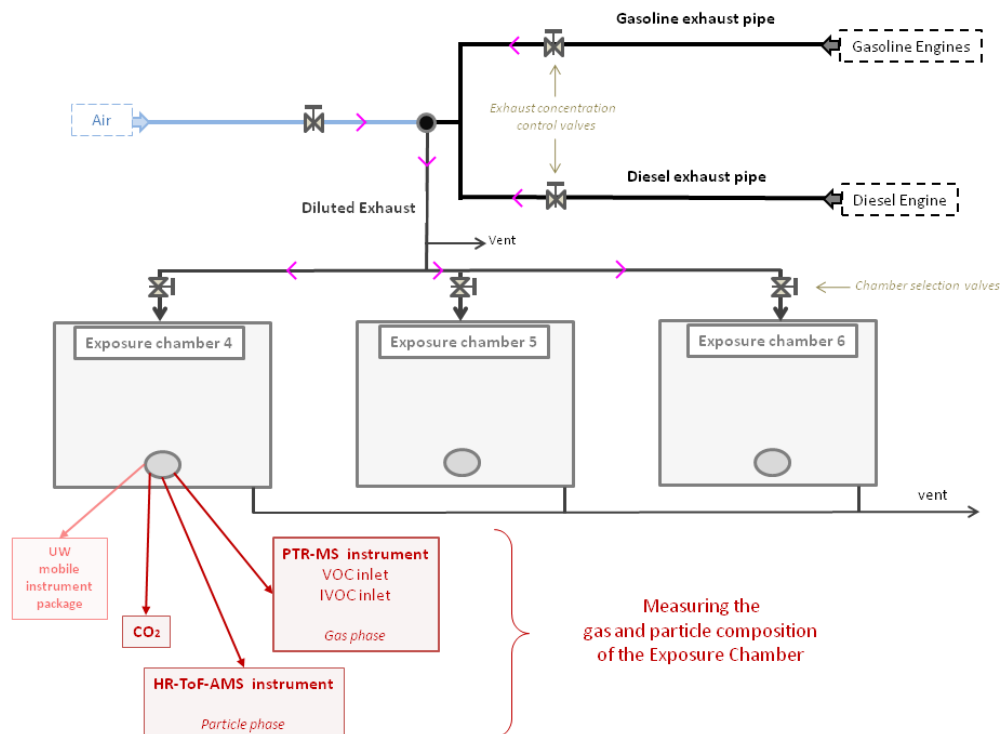


Figure 4.1. General plumbing schematic of the exposure chamber measurements

The mass loading of PM was used to determine the extent of dilution of the mixtures in the chamber. A previous study was performed on the LRRI exposure chambers (40) using the same particulate matter mass metric. The particulate load is used to represent the dilution of the exhaust. The engines were operated at different loads too. There were three types of loading: low, high and typical, all are detailed in Table 4.1. A total of 23 experiments were performed and are summarized in Table 4.2. For example, the test 90D10G_27 is a mixture of diesel and gasoline run at a typical gasoline engine load and a typical diesel engine load. The particle load is $90 \mu\text{g m}^{-3}$ for diesel and $10 \mu\text{g m}^{-3}$ for gasoline which corresponds to a dilution of 22% of the undiluted diesel exhaust and 20% of the undiluted gasoline exhaust. This test

is considered as a low particle load which represents a well diluted exhaust.

Table 4.1. Engine load conditions

Engine Loading Condition	Gas	Diesel
Typical (average)	Throttle (11%) 1123 RPM	4.5 kW
Low	Throttle (1%) 600 RPM	1.5 kW
High	Throttle (27 %) 1922 RPM	5.5 kW

Table 4.2. Experiments Summary

File name	Particle Loading ($\mu\text{g}/\text{m}^3$)		Engine Load Type
type _ date	Gas	Diesel	Gasoline : Diesel
diesel_27	0	292	\emptyset : T**
90D10G_27	12	370	T : T
gasoline_28	30	0	T : \emptyset
50D50G_m_28	50	73	T : T
50D50G_1_28*	3	4	T : T
diesel_28	0	8	\emptyset : T
gasoline_29	20	0	T : \emptyset
40D5G_29	22	10	T : T
200D25G_29	22	202	T : T
diesel_29	0	34	\emptyset : T
gasoline_30	42	0	L : \emptyset
400D50G_30	30	504	H : L
diesel_30	0	288	\emptyset : L
80D10G_30*	45	16	H : L
80D10G_01	4	114	L : H
diesel_01	0	72	\emptyset : H
400D50G_01	33	304	L : H
200D25G_02	42	236	H : H
40D50G_02*	34	52	H : H
gasoline_02*	11	0	H : \emptyset
400D50G_02	35	409	H : H
300D5G_03	10	269	H : H
gasoline_03*	24	0	H : \emptyset

* The PTR-MS signal was low and the data cannot be used for analysis.

** Engine loads: T=Typical, L=Low and H=High.

4.3 PTR-MS Sampling of Chambers

Of the 23 tests conducted, 6 tests had PTR-MS instrument problems and the data collected was not useable. The main focus of the data analysis was to compare the tests to determine the impact of engine loading and PM concentration variations on the chamber mixtures compositions. As explained in the set-up section, engine load and exhaust dilution were changed to obtain different fractional composition of diesel and gasoline in the exposure chambers. The PTR-MS used the IVOC/VOC system but only the VOC data are reported here. The air was sampled from the chambers through a heated PFA tube (1/8") and filtered with a 2 μm Teflon filter to limit the intrusion of particles into the system. Those filters were changed every experiment or chamber run. The connection to the chamber is illustrated in Figure 4.2. Selected ions were measured and were grouped into eight categories. The housekeeping ions represent the ions measured to verify that the drift tube is operating properly. The housekeeping ions were $m/z=21$, $m/z=30$, and $m/z=32$ that account for respectively H_3O^+ , NO^+ , O_2^+ , plus the $m/z=39$ and $m/z=55$ ions that correspond to the water clusters. Then, there is the alkanes $\text{C}_n\text{H}_{2n+2}$ (also called paraffins or saturated hydrocarbons) and alkenes C_nH_{2n} (also called olefin) group. It is represented by the ion series $m/z=43, 57, 71, 85, 99, 113, 127$. The PTR-MS can measure the alkanes $\geq \text{C}_{10}$ (decane) but those are likely to fragment into $m/z=43$, $m/z=57$, $m/z=71$, and the most abundant alkanes from vehicle emissions are $\leq \text{C}_{10}$ (24) so the PTR-MS does not provide representative signal for the alkanes. The alkenes $\geq \text{C}_3$ (propene) are measured by the PTR-MS and are abundant in the exhaust (24). For the exhaust measurement the ions at $m/z=43$, $m/z=57$

and $m/z=71$ are more likely to represent the alkenes more than the alkanes. The monoaromatics are represented by the $m/z=79, 93, 107, 121, 135, 149, 163, 177, 191$ ions. The tetrahydronaphthalenes group ($91 + (n*14)$) is represented by the ions at $m/z=105, 119, 133, 147, 161, 175, 189$. The naphthalenes are represented by the ions at $m/z=129, m/z=143, m/z=157$, and $m/z=171$. The PAHs are represented by the ions at $m/z=152, 155, 167$. Those were not monitored in the tests Diesel_27, Diesel_28, Gasoline_28, 50D50G_m_28, 50D50G_l_28, 90D10G_27 (see Table 4.2. There are two unknown families (C_nH_{2n-1}) and ($67 + (n*14)$) respresented by the ion series $m/z=69, 83, 97, 111, 125, 139, 153$ and $m/z=95, 109, 123, 137, 151, 165, 179$ respectively. Those ions are reported in Table 4.3.

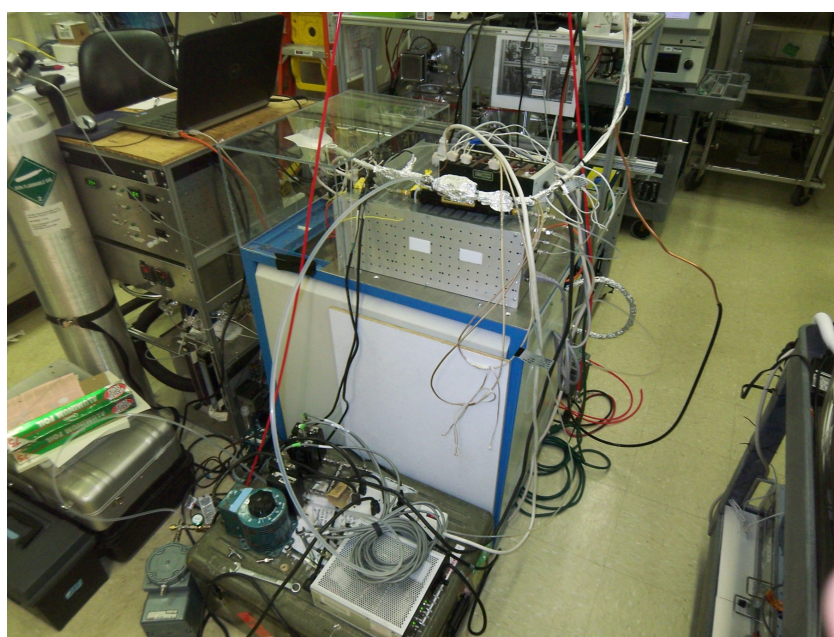
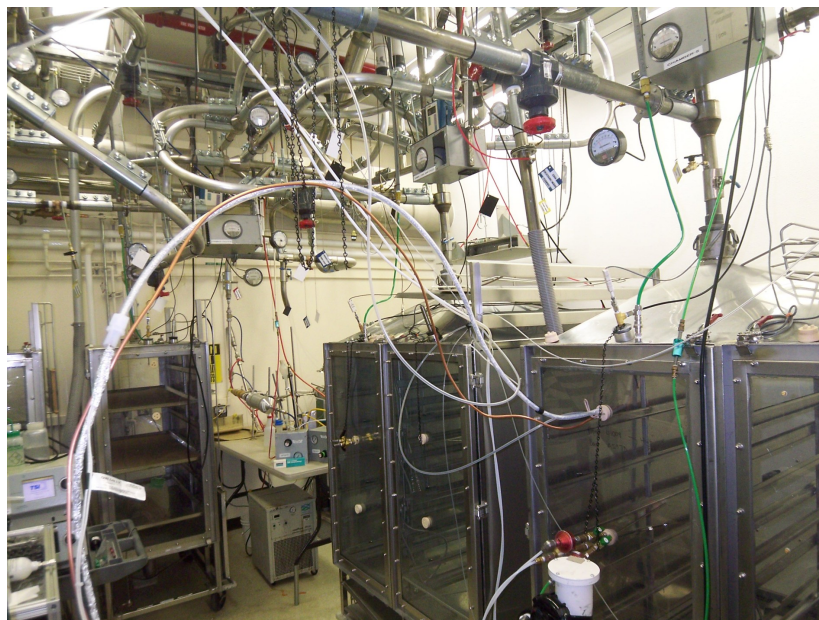


Figure 4.2. Pictures of the chamber exposure connection with the PTR-MS: Tubing sampling air from the chamber

Table 4.3. Ions measured with the PTR-MS during the exposure chamber experiment

m/z	groups	m/z	groups	m/z	groups
21	H ₃ O ⁺	81		137	67 + (n*14)
30	NO ⁺	83	C _n H _{2n-1}	139	C _n H _{2n-1}
31	HCHO	85	alkanes/alkenes	143	naphthalene
32	O ⁺	87		147	91 + (n*14)
33	methanol	93	monoaromatic	149	monoaromatic
39	Water cluster	95	67 + (n*14)	151	67 + (n*14)
41		97	C _n H _{2n-1}	152	PAHs
42		99	alkanes/alkenes	153	C _n H _{2n-1} *
43	alkanes/alkenes	101		155	PAHs **
45		105	91 + (n*14)	157	naphthalene
47		107	monoaromatic	161	91 + (n*14)
51		109	67 + (n*14)	163	monoaromatic
55	Water cluster	111	C _n H _{2n-1}	165	67 + (n*14)
57	alkanes/alkenes	113	alkanes/alkenes	167	PAHs
59		119	91 + (n*14)	171	naphthalene
61		121	monoaromatic	175	91 + (n*14)
63		123	67 + (n*14)	177	monoaromatic
65		125	C _n H _{2n-1}	179	67 + (n*14)
69	C _n H _{2n-1}	127	alkanes/alkenes	189	91 + (n*14)
71	alkanes/alkenes	129	naphthalene	191	monoaromatic
73		133	91 + (n*14)		
79	monoaromatic	135	monoaromatic		

* m/z=153 is accounting for the (C_nH_{2n-1}) group, but some PAHs may contribute to that ion mass.

** m/z=155 is accounting for the PAHs group, but some fragment ions from alkanes such as C₁₆ may contribute to that ion mass.

4.3.1 Fuels composition and comparison to engine exhaust

For both diesel and gasoline, samples of the fuel used in the Lovelace experiments were run through the PTR-MS in order to compare its composition before and after combustion. Fuels were run using the dilution system at a Td=80, with an injection

rate of $20 \mu\text{l hr}^{-1}$ and a N_2 flow of 1008 sccm. A full mass spectrum of barscans from $m/z=21$ to $m/z=215$ for diesel and from $m/z=21$ to $m/z=185$ for gasoline were measured. The diesel exhaust experiment selected for the comparison corresponds to the less diluted (i.e with an higher particle loading) diesel only and run at a low engine load which gives the highest signal: the diesel experiment from April 30th, with a particle loading of $288 \mu\text{g m}^{-3}$. For the exhaust experiments only the selected ions from Table 4.3 were measured. The comparison of the diesel exhaust mass spectrum and diesel fuel barscan is shown in Figure 4.3. The fuel has a more homogeneous composition than the exhaust with significant ion signal observed out to high mass range whereas the exhaust displays rapidly decreasing ion signal intensity at larger m/z . The diesel exhaust mass spectrum is dominated by ions from alkanes/alkenes and monoaromatics, representing respectively 26% and 19% of the total ion signal (sum of all ions measured except housekeeping). The $(\text{C}_n\text{H}_{2n-1})$ and $(67+(n*14))$ represent 4% and 2% respectively. In the fuel, the signal of alkanes/alkenes is still dominant with 30.8% of the total ion signal. The $(\text{C}_n\text{H}_{2n})$ and the monoaromatic group represent respectively 18.8% and 11.7% of the signal; the tetrahydronphthalenes and $(67+(n*14))$ are less abundant accounting for respectively 9.4% and 6.1% of the total signal. For $m/z \leq 75$, in the exhaust the alkanes/alkenes and the oxygenated ions dominate the signal and in the fuel only the alkane/alkene ions are dominant. For each group of ions from $m/z=75$ to $m/z=130$, the monoaromatics are largely dominant compared to the other organics for the exhaust but not in the fuel. For $m/z \geq 130$, in the exhaust the most abundant compounds are mainly the unknown $(67+(n*14))$ group, then the monoaromatics. In the literature Vendeuvre et al (29) measured by GCxGC the abundance of organics in diesel fuel. It appears that the

alkanes are also the most abundant group accounting for $\pm 70\%$ of the composition by mass, then the monoaromatics $\pm 18\%$, the diaromatics $\pm 10\%$ and the triaromatics $\pm 1\%$. In Han et al. (26), the diesel exhaust composition (on a lean conventional mode) was also dominated by alkanes by 27%, then alkenes 19% and aromatics 17%, those percent are with respect to HC group. The alkanes were found to be relatively more abundant in the fuel than in the exhaust.

The gasoline exhaust data selected for the comparison corresponds to the less diluted exhaust, run at a low engine load which offers the highest signal, gasoline_30. The particle loading was $42 \mu\text{g m}^{-3}$. The mass spectrums are shown in Figure 4.4. The gasoline fuel and exhaust mass spectrums are more similar than observed with diesel. Gasoline is composed of lower molecular weight alkanes and aromatics (13). Each ion group presents the same pattern, characterized by a large abundance of monoaromatics compared to the other organic families. The fuel composition is dominated by the monoaromatics representing 26% of the total ion signal. The second more abundant group is the alkanes/alkenes accounting for 9.2%. In the gasoline exhaust the monoaromatics are the most abundant representing 30% of the total ion signal, and then the alkanes/alkenes represent 25%. Schmitz et al. (30) also concluded in the dominant abundance in aromatics and alkanes, those accounting for both a volume percent of $\pm 45\%$ of their gasoline fuel. The exhaust composition was more dominated by aromatics in their study representing $\pm 50\%$ of the VOC pattern, and alkenes and alkanes both accounting for $\pm 23\%$ of the VOC pattern.

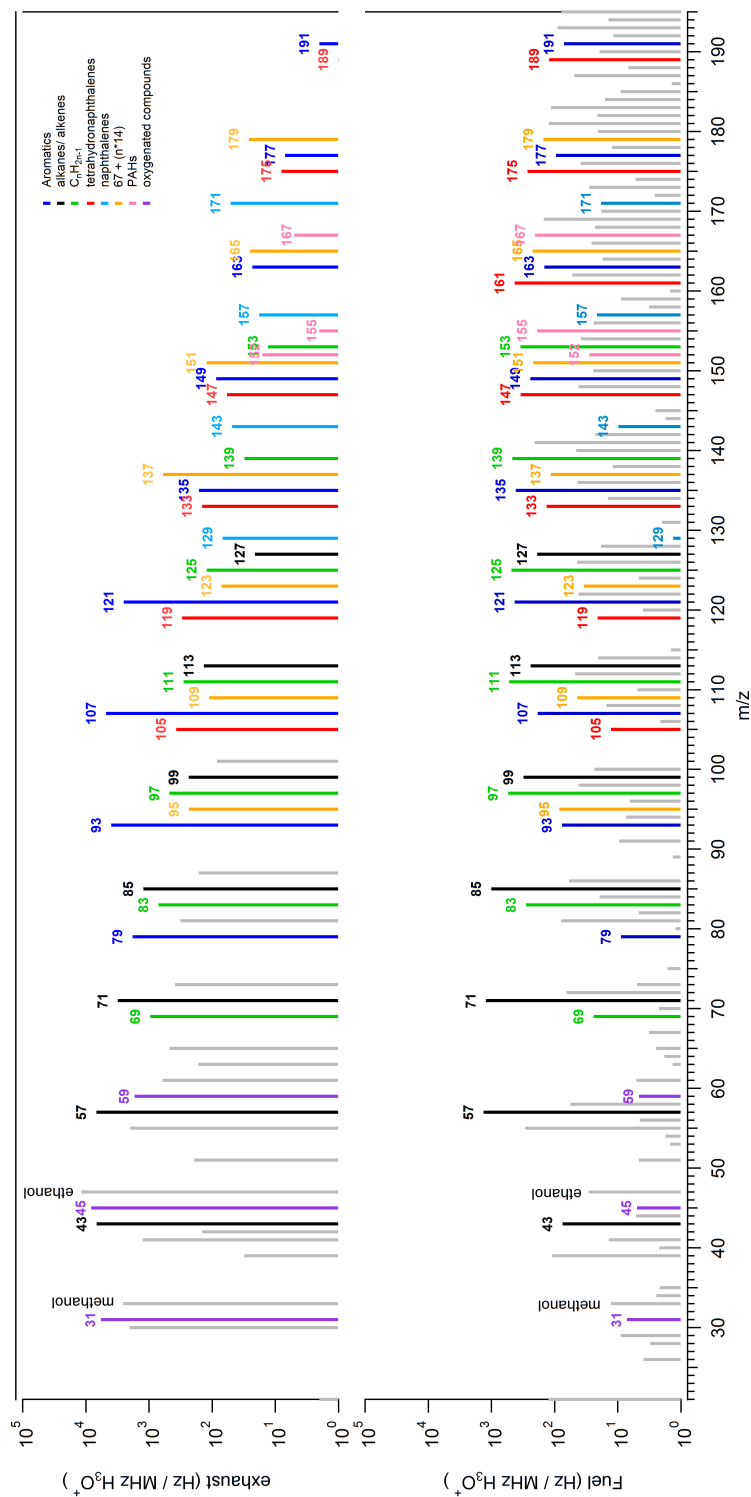


Figure 4.3. PTR-MS mass spectra of diesel exhaust (upper panel) and diesel fuel (lower panel) at Td=80. Shown are the ion count rates normalized to the reagent ion count rate in MHz. Exhaust mass spectra is color coded to group ions into chemically similar functional groups

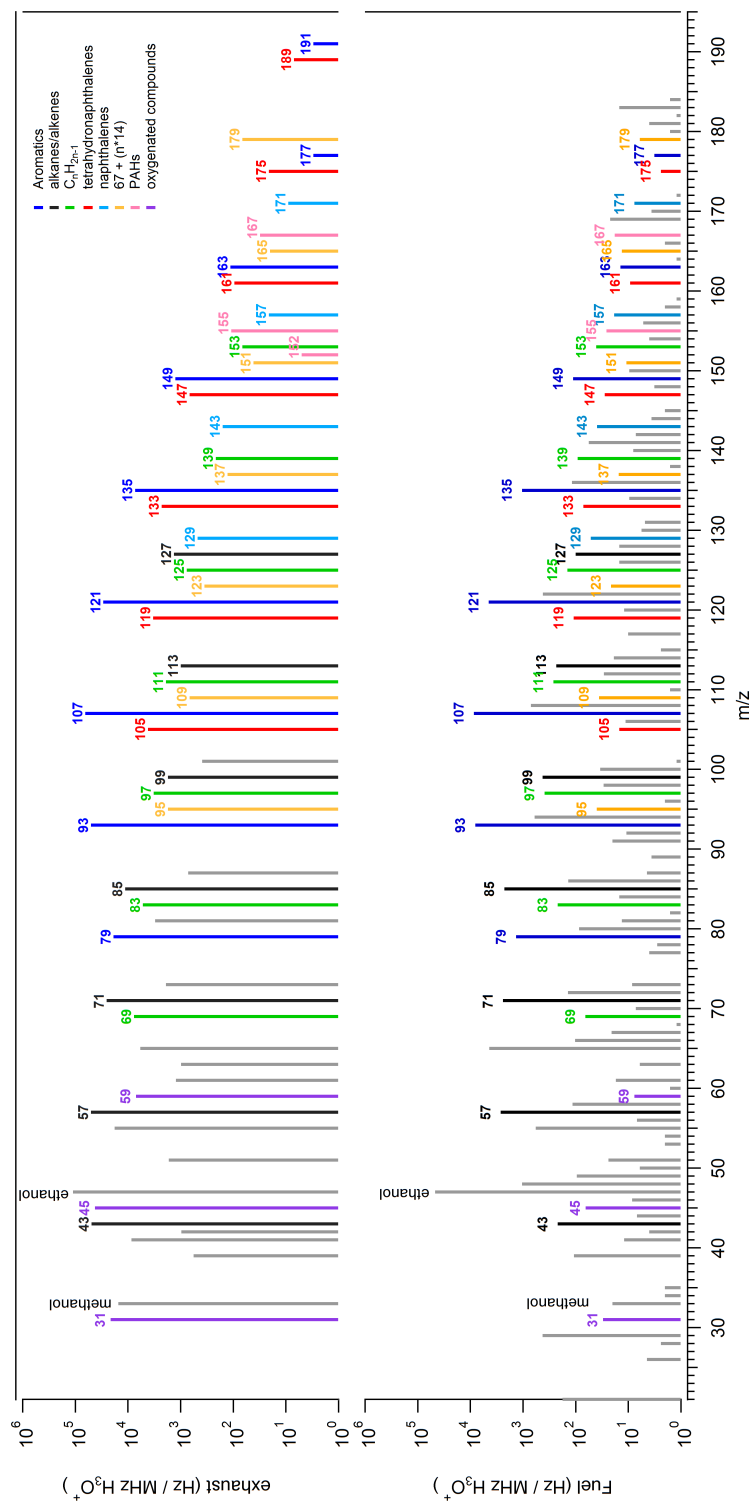


Figure 4.4. PTR-MS mass spectra of gasoline engine exhaust (upper panel) and gasoline fuel (lower panel). Shown are the ion count rates normalized to the reagent ion count rate in MHz. Exhaust mass spectra is color coded to group ions into chemically similar functional groups

4.3.2 Comparison of gasoline and diesel exhaust composition

The barscan of the diesel and gasoline fuel were really different but the exhaust mass spectrums are similar. The gasoline_30 and diesel_30 experiments (listed in Table 4.1) were selected to compare the relative abundance of organics between the two types of exhaust. The dilution for gasoline_30 was 16%, and for diesel_30 it was 28%. The diesel engine exhaust is somewhat more dilute but still allows us to draw general observations regarding compound abundance. The gasoline exhaust had higher mixing ratios of VOCs than the diesel exhaust by a factor of ≈ 10 . Although there are more organics in the gasoline exhaust, the pattern of the mass spectrums is similar for both diesel and gasoline exhaust. The abundance relative to benzene (one of the compounds of the monoaromatic family) is not too different except for the higher masses as shown on Figure 4.5. Indeed, it seems hard to distinguish with only PTR-MS measurements of the VOCs which exhaust would be diesel or gasoline because they have a similar compound distribution.

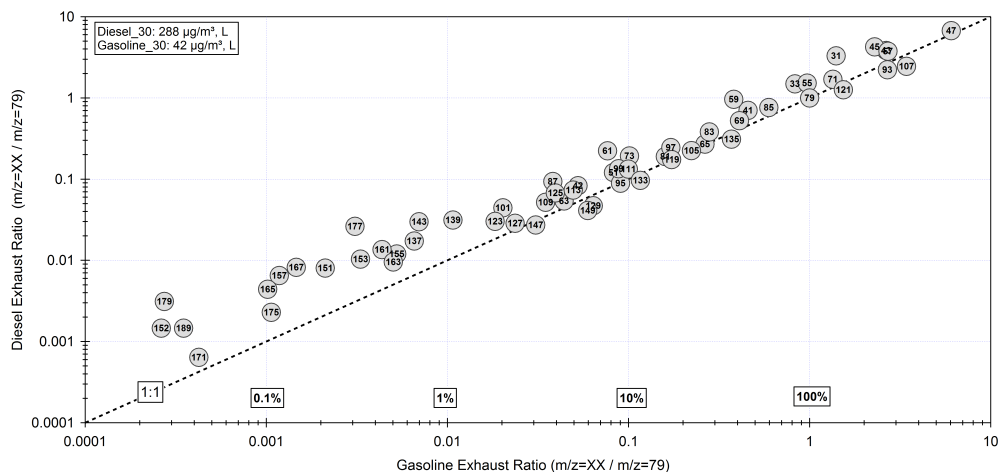


Figure 4.5. Organics abundance relative to benzene for diesel and gasoline exhaust. Numbers in circles represent the ion mass

4.3.3 Particle and engine loading variations

The set up allowed the dilution of the diesel and gasoline exhaust in order to obtain different concentrations of particles in the exposure chambers. Experiments with diesel only and gasoline only at different particle loading and engine loading were run and provide data to determine the effect of those two parameters on the gas phase composition.

4.3.3.1 Diesel

The impact of the particle loading for diesel exhaust can be studied by comparing three experiments run at a typical engine load with only a change in the particle concentration due to different dilutions. The diesel_27 experiment was run at a high particle load of $292 \mu\text{g m}^{-3}$, the diesel_29 experiment was run at a low particle load of $34 \mu\text{g m}^{-3}$ and the diesel_28 experiment was run at an even lower particle loading of only $8 \mu\text{g m}^{-3}$. The first test is expected to have a higher VOC abundance than the two other ones. The results are shown in Figure 4.6 and in Figure 4.7. The abundance of organics for all the compound groups is significantly lower in the diesel_28 test than in the two other ones as expected. The abundance is lower by a factor of four to up to fifteen depending on the group when comparing with the $34 \mu\text{g m}^{-3}$ test mixture, and by the same range except the monoaromatics when comparing with the $292 \mu\text{g m}^{-3}$ test mixture. Although we can notice that the large increase in the particle loading from $34 \mu\text{g m}^{-3}$ to $292 \mu\text{g m}^{-3}$ is not characterized by a similar increase in organic abundance, the monoaromatics are even significantly lower by a factor of 3. This could be due to the particle load that may not be representative of

the dilution method. Further analysis on the IVOC data, the CO_2 and NO_x data may provide more information to conclude on this observation.

The impact of engine load on the VOC abundance was studied using two sets of experiments. The first set compares two diesel only experiments, diesel_30 and diesel_27, that were both run at high particle load of $288 \mu\text{g m}^{-3}$ and $292 \mu\text{g m}^{-3}$ respectively but at different engine loads. The diesel_30 was run at a low engine load and the diesel_27 at a typical engine load. The results for that set are shown in Figure 4.8. The second set compares two mixtures, 400D50G_30 and 400D50G_02. For both experiments the gasoline engine load was high, the gasoline particle load was medium-high (respectively $30 \mu\text{g m}^{-3}$ and $35 \mu\text{g m}^{-3}$) and the diesel particle load was high (respectively $504 \mu\text{g m}^{-3}$ and $409 \mu\text{g m}^{-3}$), but the diesel engine load was different. The 400D50G_30 was run at a low engine load and 400D50G_02 was run at a high engine load. The second set of experiment is illustrated in 4.9. From the first set, we can see that the abundance of organics from the diesel_30 (low engine load) test is higher than the diesel_27 (typical engine load) tests by a factor of two or more for all the groups, except the naphthalenes that are very similar for both tests. The decrease in the engine loading increases the abundance of organics in the gas phase. From the second set, we can notice that the abundance of organics is significantly higher with the low diesel engine load compared to the high engine load test. PAHs increases by a factor of 4, and the other group by a factor of 10. The lower the load is, the higher the organic abundance is. The fact that the PAHs in the gas phase does not increase as much as expected could be due to some partitioning: as the diesel particles concentration increases the PAHs compounds present in the mixture are likely to condense on the particles rather than staying in the gas phase. Increasing

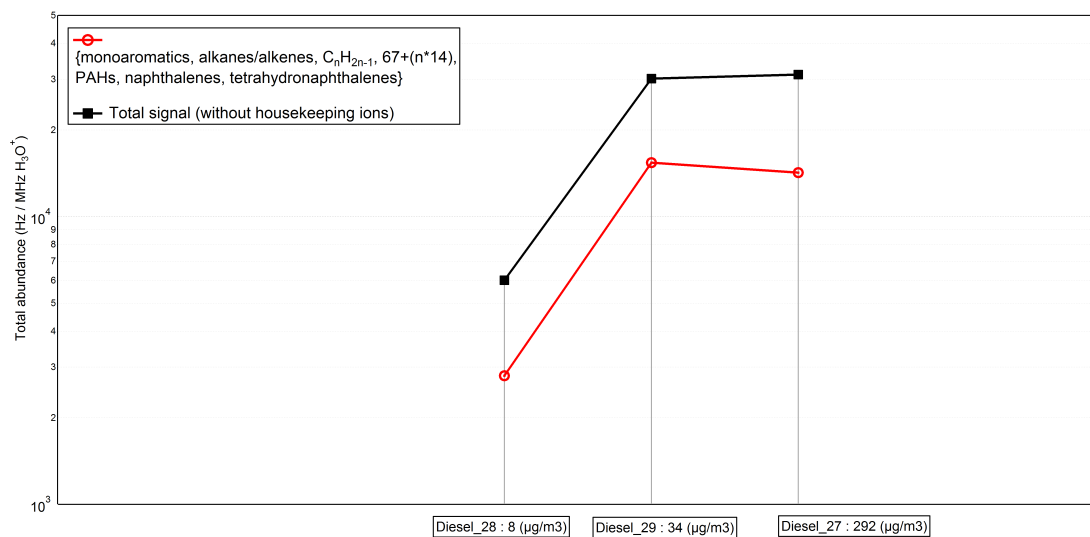


Figure 4.6. Impact of diesel particle loading on organics abundance at typical engine loading (total organic abundance).

the particle loading would enhance the partitioning. Further comparisons between the HR-ToF-AMS data and the IVOC data should provide more evidence regarding the partitioning phenomena since the IVOC inlet allows more accurate measurements of the higher molecular weight compounds as the PAHs.

4.3.3.2 Gasoline

As for diesel, the analysis of the impact of the particle load and engine load on the organic abundances was performed selecting a set of three gasoline only type of experiments: gasoline_28, gasoline_29 and gasoline_30 that were run respectively at 30 $\mu\text{g m}^{-3}$ and a typical engine load, 20 $\mu\text{g m}^{-3}$ and a typical engine load, and 42 $\mu\text{g m}^{-3}$ and a low engine load. We expect that the low dilution (higher PM concentration) and lower engine load would result in higher organic abundance in the mixture. The results are shown in Figure 4.10. We can see that for the gasoline_30

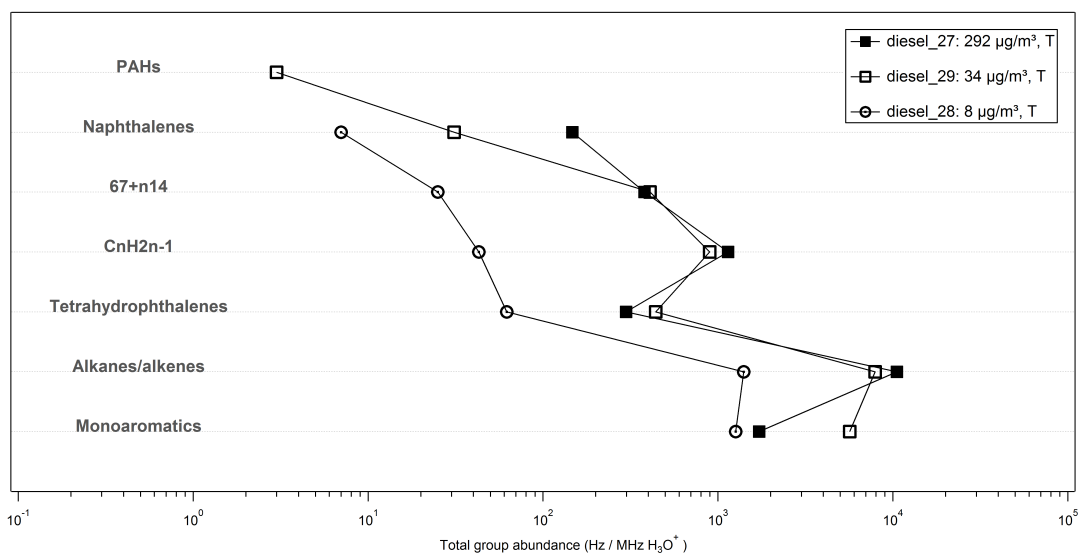


Figure 4.7. Impact of diesel particle loading on organics abundance at typical engine loading.

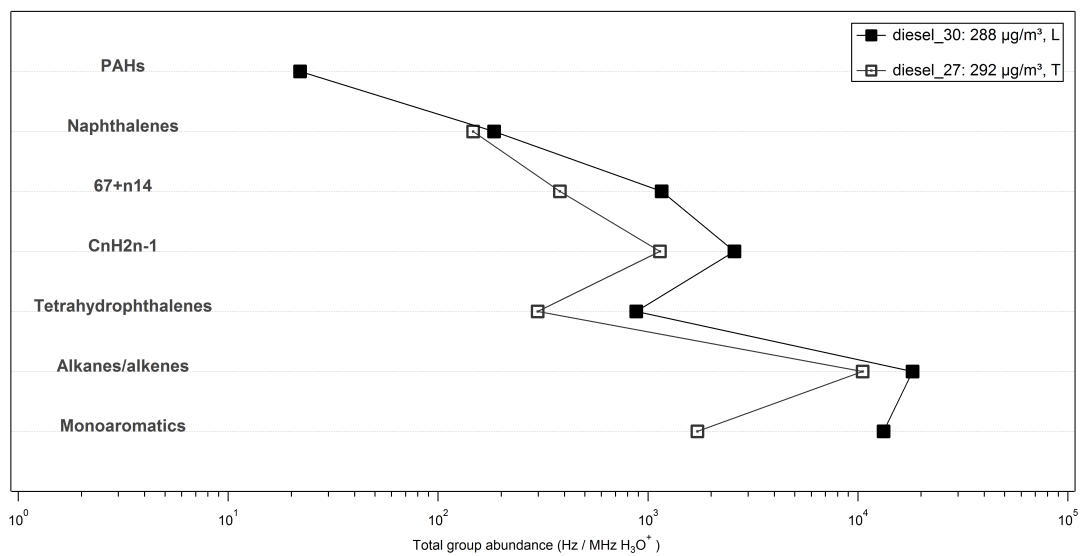


Figure 4.8. Impact of diesel engine loading on the organic abundance in a diesel only mixture, at a constant particle loading

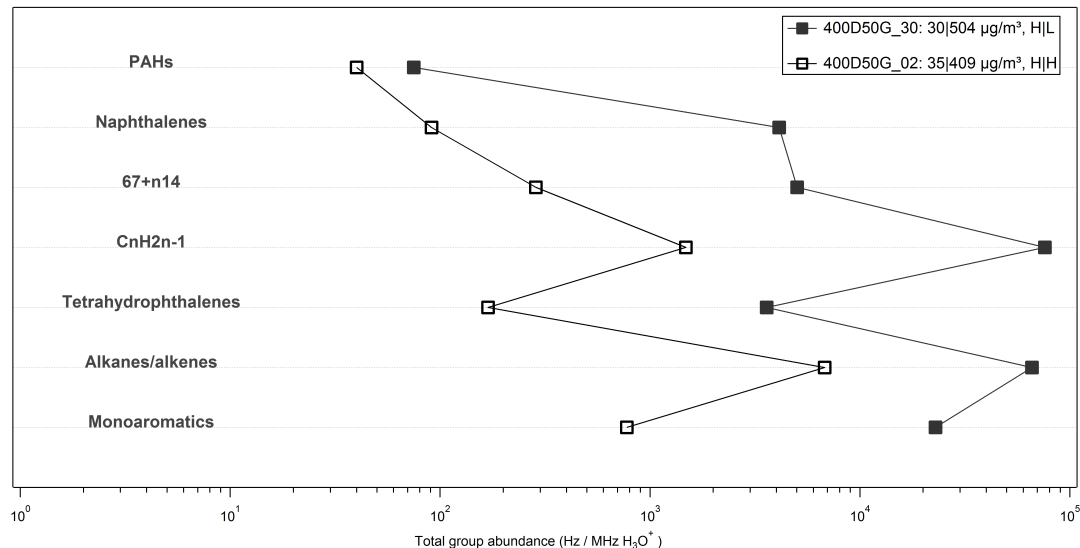


Figure 4.9. Impact of diesel engine loading on the organic abundance in a gasoline and diesel mixture, at a constant particle loading for both diesel and gasoline

test (low engine load) the organic abundance is higher than both gasoline_28 and gasoline_29 by a factor of 5 to 10 and 3 to ten respectively, depending on the group we are looking at. Similar to the diesel engine, lower engine load increases the abundance of organics.

The two typical engine loading experiments show the opposite of the expected result: as the particle concentration increases there is a decrease in the abundance of organics. This interesting observation could be explained by dilution issues that might occur so that one of those two gasoline experiments was not diluted as we thought. It also could come from a leak in the sampling plumbing that would result in lower count for the gasoline_28 so that the total abundance would be underestimated.

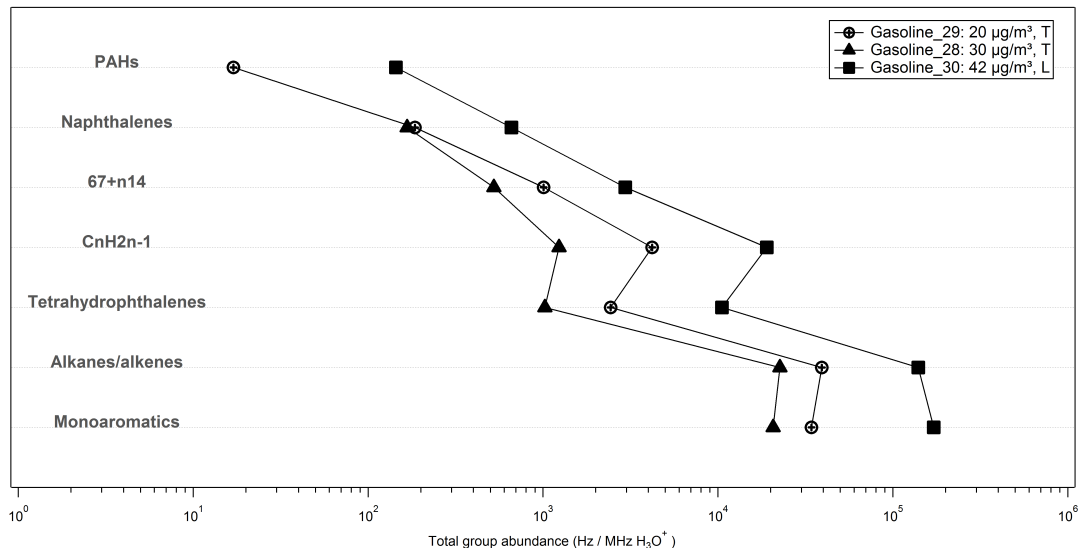


Figure 4.10. Impact of particle loading and engine loading variations for gasoline only mixtures.

4.3.3.3 Mixture with variation in the gas and particles loadings

The following three experiments were run at typical engine load and at a same gasoline particle load of $20 \mu\text{g m}^{-3}$. The variable in this set of experiments is the diesel particle load. The Gasoline_29 was only gasoline, the 45D5G_29 was a low diesel particle load of $10 \mu\text{g m}^{-3}$ and the 200D25G was a medium diesel particle load of $202 \mu\text{g m}^{-3}$. This comparison uses the VOC data to determine the variations in the gas phase, and the HR-ToF-AMS data to determine the variations in the particle phase. The particle concentration were calculated using the standard fragmentation table (41), and the collection efficiency of $\text{CE}=0.5$). There is a noticeable decrease in the organic compounds in the gas phase as the fraction of diesel (i.e the particle loading) increases. The decrease is not proportional to the fraction of diesel added because between $10 \mu\text{g m}^{-3}$ and $202 \mu\text{g m}^{-3}$ the total group abundance for the different groups of organics does not vary significantly. Increasing the fraction of diesel exhaust in the

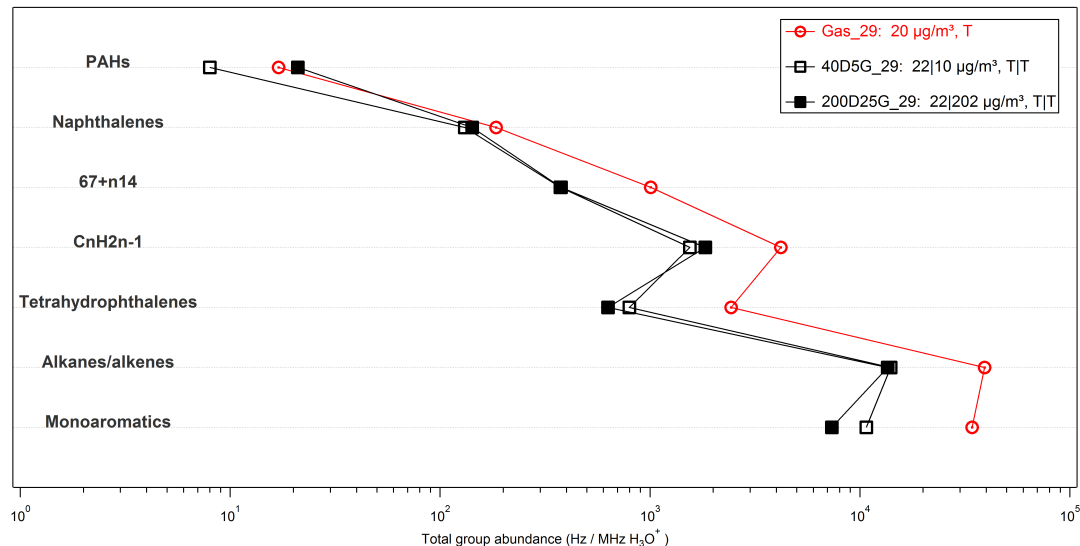


Figure 4.11. Impact of the increase in the fraction of diesel on the organic abundance of a mixture, at a constant gasoline particle load of $20 \mu\text{g m}^{-3}$ and at a typical engine loading for both diesel and gasoline.

mixture decreases the amount of VOCs in the gas phase as illustrated in Figure 4.11. A factor of decrease is barely observed for the naphthalenes and PAHs compared to the factor of 3 or more for the other families. It can be explained by the larger abundance of heavier compounds in diesel than in the gasoline. The total PM mass concentration increases significantly as the diesel fraction increases as illustrated in Figure 4.12. The total particle mass concentration includes PAHs and organic mass concentrations. This shows that the gasoline engine was the major source of VOCs and the diesel engine the major source of PM. For further analysis the comparison of the gas phase data obtained with IVOC system and the HR-ToF-AMS data could also provide evidences on the partitioning phenomena that can occur with the larger molecular weight compounds like the PAHs.

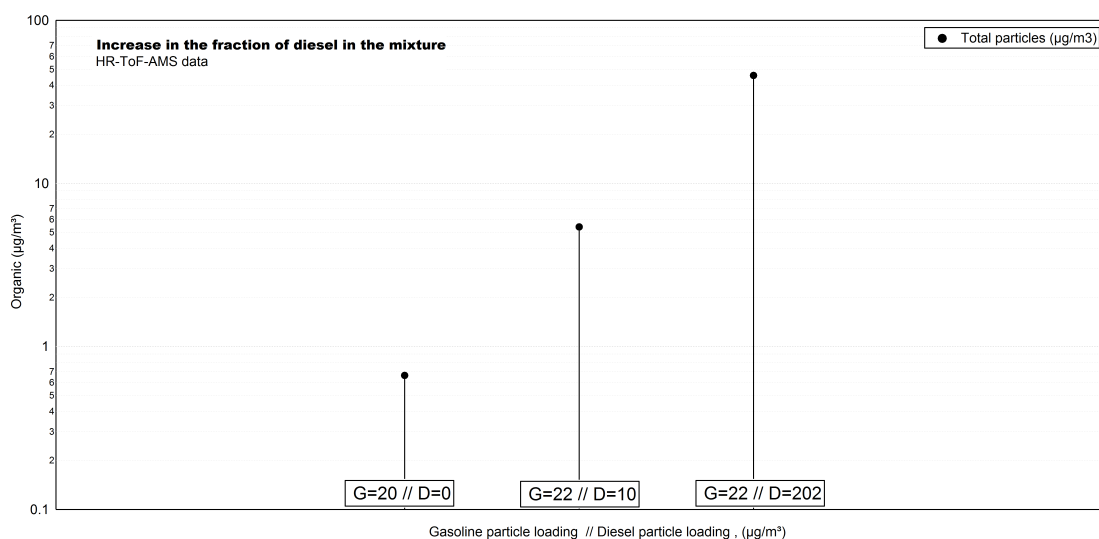


Figure 4.12. HR-ToF-AMS measurements. Impact of the increase in the fraction of diesel in the particles concentrations of a mixture, at a constant gasoline particle load of $20 \mu\text{g m}^{-3}$ and a typical engine loading for both diesel and gasoline.

CHAPTER 5. CONCLUSIONS

The first part of the laboratory experiments was to evaluate the accuracy of the dynamic dilution system. This was done by comparing mixtures made from infusing benzene, p-xylene, toluene, and 1,3,5-trimethylbenzene using the syringe pump to a test mixture made by diluting a multicomponent gas standard containing these compounds. The gas standard is what is normally used to calibrate the PTR-MS. The experiments involved varying the infusion rate from $0.1 \mu\text{l hr}^{-1}$ to $50 \mu\text{l hr}^{-1}$ as well as varying the injection manifold temperature from room temperature to 70°C . The compounds with the lower vapor pressure, p-xylene and 1,3,5-trimethylbenzene, yielded good results with less than 10% difference between the measured mixing ratio using the gas phase standard instrument sensitivity and the expected mixing ratios calculated from the infusion rate and dilution gas flow rate. The experiments with benzene and toluene suggest that injection manifold temperature needs to be adjusted to keep the compound vapor pressure below 100 Torr. At high manifold temperatures and low infusion rates, significantly more benzene and toluene ($> 20\%$) was measured than expected. Excessive mass loss due to evaporation of the liquid from the syringe needle is the likely cause. Increasing the infusion rate would mitigate this problem. This evaporative loss problem will set a limit to the lowest possible infusion rate and will be compound dependent. For future work, additional tests with other compounds

should be performed to confirm the 100 Torr upper limit and to verify the lower limit infusion rates.

Acenaphthylene, acenaphthene and biphenyl sensitivity tests were performed at Td=80 using the dynamic dilution system and resulted in normalized count rate sensitivities of respectively 3.1 ± 0.3 , 3.2 ± 0.3 and 3.2 ± 0.6 Hz per ppbV MHz H_3O^+ . These compounds did not fragment and so can be monitored at m/z=153, m/z=155, and m/z=155 respectively. The work demonstrated that it is possible to make liquid standards from these solids and measure them with the PTR-MS. The solvent used in these tests was dichloromethane. While this compound doesn't react with H_3O^+ , ions resulting from its use were observed. The ions m/z=49 and m/z=51 were attributed to the ^{35}Cl and ^{37}Cl isotopes of CH_2Cl^+ . The m/z=31 ion was also observed. Production of these ions likely resulted when air from the drift tube diffused into the ion source. For further work, these standards should be run through the thermal desorption IVOC system for comparison.

The second part of the laboratory experiments was to study fragmentation patterns of monoaromatic compounds and several polyaromatic hydrocarbons usually present in gasoline and diesel exhaust. Typically the PTR-MS is operated at Townsend numbers between 120 and 150 to avoid water cluster formation in the drift tube. Results from these experiments show that fragmentation occurs for many monoaromatic compounds at those Tds. The compounds that have ethyl groups attached to the benzene ring fragment at Td=150. Compounds with an isopropyl group attached to the benzene ring showed little fragmentation at Td=80 and high fragmentation at Td=120 and Td=150. The compounds that have a methyl group attached to the benzene ring

did not fragment. Such fragmentation patterns may produce interferences with the measurement of benzene at $m/z=79$ and toluene at $m/z=93$ in vehicle exhaust. The compounds that are composed of longer chain alkyl groups attached to the benzene ring also fragmented. It was observed that fragmentation of these compounds can produce fragment ions at $m/z=43$ and so may produce an interference with the measurement of alkanes in vehicle exhaust. The PAHs that were studied were dissolved into a dichloromethane solution. No fragmentation pattern were noticed except for the tetrahydronaphthalene that fragmented into $m/z=91$ at $T_d=150$. The laboratory experiments prove that low molecular weight PAH compounds can be measured by the PTR-MS and that these compounds have similar normalized sensitivity of 3.2 Hz per ppbV MHz H_3O^+ at $T_d=80$. For further works, some tests should be performed on additional compounds, also usually present in diesel and gasoline exhaust, to enlarge the fragmentation pattern list.

The Lovelace experiment was divided into two set of experiments. The first part focuses on the gas phase and particle phase composition of mixture of gasoline and diesel exhausts from exposure chambers. The results on the gas phase measurements by the VOC system were detailed in this thesis. The diesel fuel was composed mainly mainly of ions from the alkanes/alkenes group and made up 31% of the total ion signal. In the diesel exhaust, the alkanes/alkenes were still the most abundant group representing 26% of the total ion signal, but also contained a larger fraction of monoaromatics (19% of the total ion signal) than in the fuel (11% of the total ion signal) especially for the ion range between $m/z=75$ and $m/z=130$. The gasoline fuel was mostly composed of monoaromatics representing 26% of the total ion signal. The

gasoline exhaust composition was also dominated by aromatics representing 30% of the total ion signal, but also contained a larger fraction of alkanes/ alkenes (25% of the total ion signal) than in the fuel (9% of the total ion signal).

Experiments were run at three different engine loading: high, typical or low. Both gasoline and diesel exhaust gas phase composition was influenced by the engine loading. A decrease in the engine loading increases the abundance of the organics. For the unmixed exhaust experiments (gasoline only or diesel only) at high dilutions where PM mass concentrations were less than 8.5% of the undiluted exhaust, the change in VOC concentration was consistent with the extent of exhaust dilution as measured by the change in PM mass concentration.

Three gasoline/diesel exhaust mixtures for which the fraction of diesel increased were compared. As the fraction of diesel increased the abundance of VOC decreased for high dilution conditions (from 20 $\mu\text{g m}^{-3}$ of gasoline only to a mixture of 20 $\mu\text{g m}^{-3}$ of gasoline and 10 $\mu\text{g m}^{-3}$ of diesel). As the fraction of diesel increased the abundance of VOC remained the same for less diluted air (from 20 $\mu\text{g m}^{-3}$ of gasoline and 10 $\mu\text{g m}^{-3}$ of diesel to 20 $\mu\text{g m}^{-3}$ of gasoline and 202 $\mu\text{g m}^{-3}$ of diesel). Those results showed that the gasoline exhaust mainly contributed to the abundance of VOC in the gas phase while the diesel exhaust contributed to the particle phase.

All the data from the Lovelace experiment that were presented in this thesis were representative of the signal count but were not in mixing ratio. The next step would be to generate the results in ppbv using the sensitivities obtained during calibration tests. For further work the analysis of the IVOC data would be needed to provide additional information on the PAHs and the less volatile compounds that did not present high counts through the VOC system. The present analysis provides some

interesting evidence of gas to particle partitioning of PAH compounds, but further investigation is suggested using data from the IVOC sampling system and results from the AMS instrument.

REFERENCES

- (1) Pope CA and Dockery DW, “Health Effects of Fine Particulate Air Pollution : Lines that Connect,” *Journal of Air and Waste Management Association*, vol. 56, pp. 709–742, 2006.
- (2) Brunekreef B, Janssen NAH, de Hartog J, Harssema H, Knape M, and Van Vliet P, “Air Pollution from Truck Traffic and Lung Function in Children Living near Motorways,” *Epidemiology*, vol. 8, no. 3, pp. 298–303, 1997.
- (3) Campen MJ, Lund AK, Doyle-Eisele ML, McDonald JD, Knuckles TL, Rohr AC, Knipping EM, and Mauderly JL, “A comparison of vascular effects from complex and individual air pollutants indicates a role for monoxide gases and volatile hydrocarbons,” *Environmental health perspectives*, vol. 118, pp. 921–7, July 2010.
- (4) Cho SH, Tong H, McGee JK, Baldauf RW, Krantz QT, and Gilmour MI, “Comparative toxicity of size-fractionated airborne particulate matter collected at different distances from an urban highway,” *Environmental health perspectives*, vol. 117, pp. 1682–9, Nov. 2009.
- (5) Dockery DW, Pope CA, Xu X, Spengler JD, Ware JH, Fay ME, Benjamin G. Ferris J, and Speizer FE, “An association between air pollution and mortality

- in six U.S. cities,” *The New England Journal of Medicine*, vol. 329, no. number 24, 1993.
- (6) Dockery DW, Luttmann-Gibson H, Rich DQ, Link MS, Mittleman Ma, Gold DR, Koutrakis P, Schwartz JD, and Verrier RL, “Association of Air Pollution with Increased Incidence of Ventricular Tachyarrhythmias Recorded by Implanted Cardioverter Defibrillators,” *Environmental Health Perspectives*, vol. 113, pp. 670–674, Feb. 2005.
 - (7) Gilmour MI, McGee J, Duvall RM, Dailey L, Daniels M, Boykin E, Cho SH, Doerfler D, Gordon T, and Devlin RB, “Comparative toxicity of size-fractionated airborne particulate matter obtained from different cities in the United States.,” *Inhalation toxicology*, vol. 19(Suppl.1, pp. 7–16, Jan. 2007.
 - (8) McDonald JD, Reed MD, Campen MJ, Barrett EG, Seagrave J, and Mauderly JL, “Health effects of inhaled gasoline engine emissions.,” *Inhalation toxicology*, vol. 19 Suppl 1, pp. 107–16, Jan. 2007.
 - (9) Peters A, Von Klot S, Heier M, Trentinaglia I, Hörmann A, Wichmann HE, and Löwel H, “Exposure to Traffic and the Onset of Myocardial Infarction,” *The New England Journal of Medicine*, vol. 351, no. 17, pp. 1721–1730, 2004.
 - (10) Seagrave J, McDonald JD, Gigliotti AP, Nikula KJ, Seilkop SK, Gurevich M, and Mauderly JL, “Mutagenicity and in vivo toxicity of combined particulate and semivolatile organic fractions of gasoline and diesel engine emissions.,” *Toxicological sciences*, vol. 70, pp. 212–26, Dec. 2002.
 - (11) Lai C, Chen K, Ho Y, and Chou M, “Characteristics of C2-C15 hydrocarbons

- in the air of urban Kaohsiung, Taiwan,” *Atmospheric Environment*, vol. 38, pp. 1997–2011, Apr. 2004.
- (12) Schauer JJ, Kleeman MJ, Cass GR, and Simoneit BRT, “Measurement of Emissions from Air Pollution Sources. 5. C1-C32 Organic Compounds from Gasoline-Powered Motor Vehicles,” *Environmental Science & Technology*, vol. 36, pp. 1169–1180, 2002.
 - (13) Zielinska B, Sagebiel JC, Harshfield G, Gertler AW, and Pierson WR, “Volatile Organic compounds up to C20 emitted from motor vehicles; measurement methods,” *Atmospheric Environment*, vol. 30, no. 12, pp. 2269–2286, 1996.
 - (14) Rogge WF, Hildemann LM, Mazurek MA, and Cass GR, “Mathematical modeling of atmospheric fine particle-associated primary organic compound concentrations,” 1996.
 - (15) Robinson AL, Donahue NM, Shrivastava MK, Weitkamp Ea, Sage AM, Grieshop AP, Lane TE, Pierce JR, and Pandis SN, “Rethinking organic aerosols: semivolatile emissions and photochemical aging,” *Science*, vol. 315, pp. 1259–62, Mar. 2007.
 - (16) Presto A, Miracolo M, Kroll JH, Worsnop DR, Robinson AL, and Donahue NM, “Intermediate-volatility organic compounds: a potential source of ambient oxidized organic aerosol,” *Environmental Science & Technology*, vol. 43, pp. 4744–9, July 2009.
 - (17) Odum JR, Hoffmann T, Bowman F, Collins D, Flagan RC, and Seinfeld JH,

- “Gas/Particle Partitioning and Secondary Organic Aerosol Yields,” *Environmental Science & Technology*, vol. 30, pp. 2580–2585, Jan. 1996.
- (18) Seinfeld JH and Pandis SN, *Atmospheric Chemistry and Physics: From Air Pollution to Climate Change*. Wiley-Interscience, 2006.
- (19) de Gouw J and Warneke C, “Measurements of volatile organic compounds in the earth’s atmosphere using proton-transfer-reaction mass spectrometry,” *Wiley Periodicals, Inc*, vol. 26, pp. 223–257, 2007.
- (20) Dasgupta PK, Li J, Zhang G, Luke WT, McClenny WA, Stutz J, and Fried A, “Summertime Ambient Formaldehyde in Five U.S. Metropolitan Areas: Nashville, Atlanta, Houston, Philadelphia, and Tampa,” *Environmental Science & Technology*, vol. 39, pp. 4767–4783, July 2005.
- (21) Cogliano V, Grosse Y, Baan R, Straif K, Secretan B, and Ghissassi FE, “Advice on formaldehyde and glycol ethers,” *The Lancet Oncology*, vol. 5, p. 528, Sept. 2004.
- (22) Mohamed MF, Kang D, and Aneja VP, “Volatile organic compounds in some urban locations in United States,” *Chemosphere*, vol. 47, pp. 863–882, June 2002.
- (23) Ho KF, Lee SC, Ho WK, Blake DR, Cheng Y, Li YS, Ho SSH, Fung K, Louie PKK, and Park D, “Vehicular emission of volatile organic compounds (VOCs) from a tunnel study in Hong Kong,” *Atmospheric Chemistry and Physics*, vol. 9, pp. 7491–7504, Oct. 2009.
- (24) Lough GC, Schauer JJ, Lonneman Wa, and Allen MK, “Summer and winter nonmethane hydrocarbon emissions from on-road motor vehicles in the Mid-

- western United States.,” *Journal of the Air & Waste Management Association*, vol. 55, pp. 629–46, May 2005.
- (25) McGaughey GR, Desai NR, Allen DT, Seila RL, Lonneman Wa, Fraser MP, Harley Ra, Pollack AK, Ivy JM, and Price JH, “Analysis of motor vehicle emissions in a Houston tunnel during the Texas Air Quality Study 2000,” *Atmospheric Environment*, vol. 38, pp. 3363–3372, June 2004.
- (26) Han M, Assanis DN, Jacobs TJ, and Bohac SV, “Method and Detailed Analysis of Individual Hydrocarbon Species From Diesel Combustion Modes and Diesel Oxidation Catalyst,” *Journal of Engineering for Gas Turbines and Power*, vol. 130, no. 4, p. 042803, 2008.
- (27) Siegl W, Hammerle H, Hermann H, Wenclawiak B, and Luers-Jonge B, “Organic emissions profile for a light-duty diesel vehicle,” *Atmospheric Environment*, vol. 33, pp. 797–805, Feb. 1999.
- (28) Schauer J, Kleeman M, Cass GR, and Simoneit BRT, “Measurement of emissions from air pollution sources. 2. C1 through C30 organic compounds from medium duty diesel trucks,” *Science & Technology*, vol. 33, no. 10, pp. 1578–1587, 1999.
- (29) Vendeuvre C, Ruiz-Guerrero R, Bertoncini F, Duval L, Thiébaud D, and Hennion MC, “Characterisation of middle-distillates by comprehensive two-dimensional gas chromatography (GCxGC): A powerful alternative for performing various standard analysis of middle-distillates,” *Journal of Chromatography A*, vol. 1086, pp. 21–28, Sept. 2005.
- (30) Schmitz T, Hassel D, and Weber FJ, “Determination of VOC-components in

- the exhaust of gasoline and diesel passenger cars,” *Atmospheric Environment*, vol. 34, pp. 4639–4647, Jan. 2000.
- (31) Lindinger W, Hansel A, and A. Jordan , “On-line monitoring of volatile organic compounds at pptv levels by means of Proton-Transfer-Reaction Mass Spectrometry (PTR-MS) Medical applications, food control and environmental research,” *International Journal of Mass Spectrometry*, vol. 173, pp. 191–241, 1998.
 - (32) Jobson BT and McCoskey JK, “Sample drying to improve HCHO measurements by PTR-MS instruments: laboratory and field measurements,” *Atmospheric Chemistry and Physics*, vol. 10, pp. 1821–1835, Feb. 2010.
 - (33) Faiola CL, Erickson MH, Fricaud VL, Jobson BT, and VanReken TM, “Quantification of biogenic volatile organic compounds with a flame ionization detector using the effective carbon number concept,” *Atmospheric Measurement Techniques*, vol. 5, pp. 1911–1923, Aug. 2012.
 - (34) Buhr K, van Ruth S, and Delahunty C, “Analysis of volatile flavour compounds by Proton Transfer Reaction-Mass Spectrometry: fragmentation patterns and discrimination between isobaric and isomeric compounds,” *International Journal of Mass Spectrometry*, vol. 221, pp. 1–7, Nov. 2002.
 - (35) Jobson B, Alexander M, Maupin G, and Muntean G, “On-line analysis of organic compounds in diesel exhaust using a proton transfer reaction mass spectrometer (PTR-MS),” *International Journal of Mass Spectrometry*, vol. 245, pp. 78–89, Aug. 2005.

- (36) Barker J, *Mass Spectrometry: Analytical Chemistry by Open Learning*. Wiley, 1999.
- (37) Foureman G, “Concise International Chemical Assessment Document 18: CUMENE,” tech. rep., WorldHealthOrganization, Research Triangle Park, NC, USA, 2005.
- (38) McLafferty FW and Turecek F, *Interpretation of Mass Spectra*. University Science Books, Mill Valley, California, 4th ed., June 1994.
- (39) McDonald JD, Campen MJ, Harrod KS, Seagrave J, Seilkop SK, and Mauderly JL, “Engine-operating load influences diesel exhaust composition and cardiopulmonary and immune responses,” *Environmental health perspectives*, vol. 119, pp. 1136–41, Aug. 2011.
- (40) McDonald JD, Barr EB, White RK, Chow JC, Schauer JJ, Zielinska B, and Grosjean E, “Generation and characterization of four dilutions of diesel engine exhaust for a subchronic inhalation study,” *Environmental Science & Technology*, vol. 38, pp. 2513–22, May 2004.
- (41) Allan JD, Delia AE, Coe H, Bower KN, Alfarra M, Jimenez JL, Middlebrook AM, Drewnick F, Onasch TB, Canagaratna MR, Jayne JT, and Worsnop DR, “A generalised method for the extraction of chemically resolved mass spectra from Aerodyne aerosol mass spectrometer data,” *Journal of Aerosol Science*, vol. 35, pp. 909–922, July 2004.